nature immunology

Article

https://doi.org/10.1038/s41590-025-02416-z

CD38 endows local antigen-specific T_{reg} cells with stress resilience for control of compartmentalized CNS inflammation

Received: 17 August 2025

Accepted: 31 December 2025

Published online: 29 January 2026

Check for updates

Hsin-Hsiang Chen[1], Sofia Tyystjärvi[1], Diego Ruiz Navarro[1], Ravi Kant[2], Tanja Groll[3], Ingrid Wagner[4], Helena Domínguez Moreno[1], Irene Bonafonte-Pardàs[5], Rupert Öllinger[6], Ali Maisam Afzali[1,7], Sylvia Heink[1], Lisa Charlotte Richter[1], Christopher Sie[1], Gildas Lepennetier[1], Lea Seeholzer[1], Katja Steiger[3], Doron Merkler[4], Roland Rad[6], Gunnar Schotta[8], Benjamin Schubert[5], Andreas Muschaweckh[1,10] & Thomas Korn[1,7,9,10]

Foxp3-expressing regulatory T (T_{reg}) cells protect against systemic autoimmunity. However, little is known about the significance of T_{reg} cells in inflammation-experienced tissues. Here, we use an experimental autoimmune encephalomyelitis model and show that T_{reg} cells accumulate and persist in the central nervous system (CNS) long after the resolution of the bulk of the inflammatory infiltrate. CNS-specific depletion of postinflammatory T_{reg} cells, but not systemic depletion of T_{reg} cells, results in autoimmune inflammatory flares in the CNS by residual local effector T cells. Expression of the NAD-consuming ectoenzyme CD38 is crucial for the functional adaptation of postinflammatory CNS T_{reg} cells to a stressful microenvironment, in which access to interleukin-2 (IL-2) is limited. CD38 counteracts ADP-ribosylation of the IL-2 receptor and thus maintains its high sensitivity to IL-2. This fully functional high-affinity IL-2 receptor prevents the loss of tissue-resident antigen-specific T_{reg} cells. These 'stress-tolerant' CNS T_{reg} cells impede the collapse of immune homeostasis in the CNS once acute inflammation is controlled.

Foxp3$^+$ regulatory T (T_{reg}) cells have regained attention due to their ability to adapt to tissue niches and exert noncanonical functions in tissue homeostasis and regeneration[1,2]. Although the developmental trajectory of tissue-resident T_{reg} cells is consistent with a thymic origin of these cells in most tissues, peripherally induced T_{reg} cells might be prevalent in some barrier-associated tissues with a high load of commensal microbiota[3]. A widely accepted model of tissue T_{reg} cell development suggests a multistep process, involving the imprinting of a tissue T_{reg} cell precursor subset in secondary lymphoid tissue and the terminal instruction to tissue T_{reg} cells by the specific milieu in the target tissue[4,5]. The dwell time of T_{reg} cells in nonlymphoid tissues may vary depending on the tissue context[6], and egress of T_{reg} cells from these tissues, rejoining the circulation, may occur[7]. However, the description of T_{reg} cell population dynamics and functional phenotype has mostly been performed in the steady state[8,9]. It is unclear how T_{reg} cells behave in nonlymphoid tissues with low-grade chronic inflammation, as is observed in most autoimmune diseases, including multiple sclerosis.

It is well established that T_{reg} cells are essential in re-establishing immune homeostasis in any adaptive immune response, where IL-2-driven feedforward loops lead to the expansion of effector T cells[10]. Once autoimmune inflammation in the central nervous system (CNS) has been initiated, thymus-derived T_{reg} cells are recruited to the CNS[11]. In

A full list of affiliations appears at the end of the paper. e-mail: thomas.korn@tum.de

the target tissue, they adopt an effector phenotype, which is steered by a network of transcription factors, including BLIMP1 and BATF[12–14]. This transcriptional network also secures the preservation of T_{reg} cell identity in the face of inflammation. Because highly activated effector T cells are resilient to T_{reg} cell-mediated control[11], it has been suggested that conventional T cell-intrinsic down-modulatory mechanisms must be initiated before efficient T_{reg} cell-mediated suppression can take effect.

T_{reg} cells that accumulate in the CNS in autoimmune inflammatory diseases (but also after stroke, in traumatic brain injury and perhaps even neurodegenerative diseases) were suggested to be involved in tissue repair and regulation of organ function by a series of different mechanisms[15–20]. The relevance of Foxp3$^+$ T_{reg} cells for these processes has been demonstrated in loss- and gain-of-function approaches. However, whether T_{reg} cells that accumulate in the CNS after the peak of experimental autoimmune encephalomyelitis (EAE; a paradigmatic model for autoimmune CNS disease) actually contribute to the re-establishment and subsequent maintenance of immune homeostasis in the CNS is not known. The postinflammatory CNS is a hostile environment for T_{reg} cells, as it is low in interleukin-2 (IL-2) due to the contraction of the conventional T (T_{conv}) cell compartment and simultaneously holds high levels of nicotinamide adenine dinucleotide (NAD^+)[21]. High levels of extracellular NAD^+ have been shown to induce apoptosis in T_{reg} cells, in part by facilitating the ADP-ribosylation of the ATP-gated ion channel $P2RX_7$ (ref. 22), which induces a gain-of-function of this molecule with a downstream increase in intracellular Ca^{2+} (ref. 23). Nevertheless, Foxp3$^+$ T_{reg} cells constitute a stable population in the postinflammatory CNS.

Here, we show that the NAD^+ consuming enzyme CD38 controls stress resilience of CNS-resident T_{reg} cells by preventing ADP-ribosylation and subsequent loss of function of the IL-2 receptor α-subunit (IL-2Rα; CD25). This function enables CNS T_{reg} cells to survive despite a limited amount of IL-2 in the microenvironment and to exert compartmentalized immune control in the inflammation-experienced CNS.

Results

T_{reg} cells persist in the CNS after recovery from an autoimmune response

To investigate the population dynamics and function of T_{reg} cells in the CNS during recovery from autoimmune inflammation, we used the $MOG_{35–55}$-induced EAE model in *Foxp3* (green fluorescent protein (GFP)) reporter mice[24]. After an acute monophasic inflammatory episode, $MOG_{35–55}$-induced EAE is characterized by a prolonged period of recovery, during which clinical symptoms improve and stabilize but usually never fully resolve (Fig. 1a). Although the neurological sequelae in this model are due to incomplete recovery from axonal damage caused during the acute phase of the disease, the inflammatory infiltrate in the CNS in the recovery phase is largely reduced. Here, we focused on this 're-established' homeostatic condition in recovery and interrogated the CNS T_{reg} cell compartment.

Although T_{conv} cell numbers declined significantly between the peak and early recovery phase (Fig. 1b,c), T_{reg} cell numbers remained largely stable during this time frame in both the brain and spinal cord (Fig. 1b,d). Consequently, the local frequency of T_{reg} cells within the CNS CD4$^+$ T cell compartment increased significantly in the postinflammatory CNS (Fig. 1d). Notably, T_{reg} cells persisting in the postinflammatory CNS were not evenly distributed but were located in certain niches around the third ventricle and in the meningeal space (Extended Data Fig. 1).

To gauge the contribution of the systemic immune compartment to the CNS T_{reg} cell pool, we labeled mitoDendra2-expressing T cells in the draining lymph nodes of MOG-immunized mice at the peak of EAE and during recovery (day 30) and tracked photoconverted T cells to the spleen and CNS (Fig. 1e). Although CD4$^+$ T cells still trafficked to the CNS during peak disease, the recruitment of T cells from the initial priming site to the CNS significantly dropped during recovery (Fig. 1f) and was negligible for T_{reg} cells (Fig. 1g). Conversely, the fraction of proliferating CNS T_{reg} cells was about 10% at the peak of EAE and dropped to 3% in the postinflammatory CNS (Fig. 1h,i). Together, these data suggest that the T_{reg} cell pool in the postinflammatory CNS was essentially disconnected from its priming site in the systemic immune compartment and, to some extent, had self-renewing capacity.

To investigate the stability of postinflammatory T_{reg} cells in their CNS environment, we used *Foxp3*$^{Cre\text{-}ERT2}$ × *Rosa26*$^{LSL\text{-}tdTomato}$ mice to perform fate mapping of Foxp3$^+$ T_{reg} cells. Tamoxifen was administered at EAE recovery (Fig. 1j). This allowed us to categorize T_{reg} cells into stable (*Foxp3* (GFP)$^+$tdTomato$^+$) and unstable (*Foxp3* (GFP)$^-$tdTomato$^+$) populations. We termed those T_{reg} cells that persisted as stable Foxp3 expressors in inflammation-experienced tissues 'stress-tolerant' T_{reg} cells. Notably, most CNS T_{reg} cells maintained stable Foxp3 expression in the recovery phase, with only 15 to 20% of CNS T_{reg} cells losing Foxp3 expression (Fig. 1k). To identify potential drivers of instability in recovery CNS T_{reg} cells, RNA-sequencing (RNA-seq) analysis was performed in stable and unstable T_{reg} cell populations isolated during the recovery phase (Extended Data Fig. 2a,b and Supplementary Tables 1 and 2). Stress-tolerant T_{reg} cells expressed key immunosuppressive molecules, including *Il2rb*, *Ctla4* and *Areg*. Conversely, unstable T_{reg} cells exhibited increased expression of *Bach2*, a transcription factor known to reduce Foxp3 expression[25], and *Tcf7*, which suppresses the transcription of genes co-bound by Foxp3 (ref. 26). These findings suggest that the

Fig. 1 | T_{reg} cells persist in the CNS in chronic EAE. a, Mean EAE scores + s.e.m. (sample sizes as in **c** and **d**) in *Foxp3* (GFP) mice following immunization. Naive (without immunization), preonset (day 8 after immunization), peak (day 15 after immunization) and recovery (day 29 after immunization). **b**, Cytograms with percentages of T_{conv} (CD3$^+$CD4$^+$Foxp3$^-$) and T_{reg} (CD3$^+$CD4$^+$Foxp3$^+$) cells among total CD4$^+$ T cells in the brain and spinal cord. **c**,**d**, Fractions and absolute (Abs.) counts of T_{conv} (**c**) and T_{reg} cells (**d**) in the brain. Open symbols represent individual mice. Data are shown as mean + s.d. *P* values in **c** and **d** are from a two-way analysis of variance (ANOVA) with a Tukey's honestly significant difference (HSD) test (naive $n = 5$, preonset $n = 4$, peak $n = 3$, recovery $n = 3$ biological replicates). **e**, EAE was induced in *Cd4*^{Cre} × *Rosa26*$^{LSL\text{-}mitoDendra2}$ mice, and inguinal lymph nodes (iLNs) were photoconverted at peak or during recovery. Two days later, photoconverted mitoDendra2^{RED} (mD^{RED}) CD4$^+$ T cells were analyzed in the spleen (SPL) and CNS. **f**, Cytograms of the CD4$^+$ T cell compartment with the fraction of photoconverted cells (%). In the bar graphs, each symbol represents an individual mouse. Data are shown as mean + s.d. *P* values are from an unpaired two-tailed Student's *t*-test (peak $n = 6$, recovery $n = 10$ biological replicates). **g**, Photoconverted CNS T_{conv} (CD4$^+$CD25$^-$GITR$^-$mD^{RED+}) and T_{reg} (CD4$^+$CD25$^+$GITR$^+$mD^{RED+}) cells were quantified. Each symbol represents an individual mouse. Data are shown as mean + s.d. *P* values are from an unpaired two-tailed Student's *t*-test ($n = 3$ biological replicates). **h**, In vivo EdU incorporation was measured in C57BL/6 wild-type EAE mice at peak and during recovery. **i**, Gating was performed on extravascular (CD45.2$^-$) near-IR dead$^-$CD4$^+$ T cells. The percentages of EdU$^+$ T_{conv} (Foxp3$^-$) and T_{reg} (Foxp3$^+$) cells were quantified. Symbols represent individual mice. Data are shown as mean + s.d. *P* values are from a two-way ANOVA with a Tukey's HSD test (peak $n = 4$, recovery $n = 3$ biological replicates). **j**, In vivo Foxp3 fate mapping was conducted in *Foxp3*$^{Cre\text{-}ERT2}$ × *Rosa26*$^{LSL\text{-}tdTomato}$ EAE mice. Mice were injected with tamoxifen (i.p.) for 5 days at the EAE recovery stage, and CNS cells were analyzed 14 days after the last injection. **k**, Representative cytogram with percentages of stable (Foxp3 (GFP)$^+$tdTomato$^+$) and unstable (Foxp3 (GFP)$^-$tdTomato$^+$) T_{reg} cells within the CNS CD4$^+$ T cell gate during EAE recovery. **l**, Stable and unstable CNS T_{reg} cells were sorted and analyzed by bulk RNA-seq ($n = 5$ biological replicates). An enrichment plot for 'IL-2–STAT5 signaling' derived from GSEA comparing stable and unstable CNS T_{reg} cells is shown; FDR, false discovery rate; NES, normalized enrichment score. **m**, CD25 expression of stable and unstable CNS T_{reg} cells at the recovery phase. Each symbol represents an individual mouse. Data are shown as mean + s.d. *P* are values from a paired two-tailed Student's *t*-test ($n = 3$ biological replicates); MFI, mean fluorescence intensity.

https://doi.org/10.1038/s41590-025-02416-z

downregulation of Foxp3 in unstable T_{reg} cells is linked to the activity of *Bach2* and *Tcf7*. By contrast, the dominant pathway associated with CNS T_{reg} cell stability in the postinflammatory CNS was the 'IL-2–STAT5 signaling' pathway (Fig. 1l and Extended Data Fig. 2c). To confirm our RNA-seq findings in stress-tolerant T_{reg} cells, we analyzed the expression of IL-2Rα (CD25) in stable and unstable T_{reg} cells using flow cytometry. Consistent with the transcriptomic data, IL-2Rα expression was significantly lower in unstable than in stable CNS T_{reg} cells (Fig. 1m), further highlighting the strong association between IL-2 signaling and Foxp3 stability in stress-tolerant T_{reg} cells.

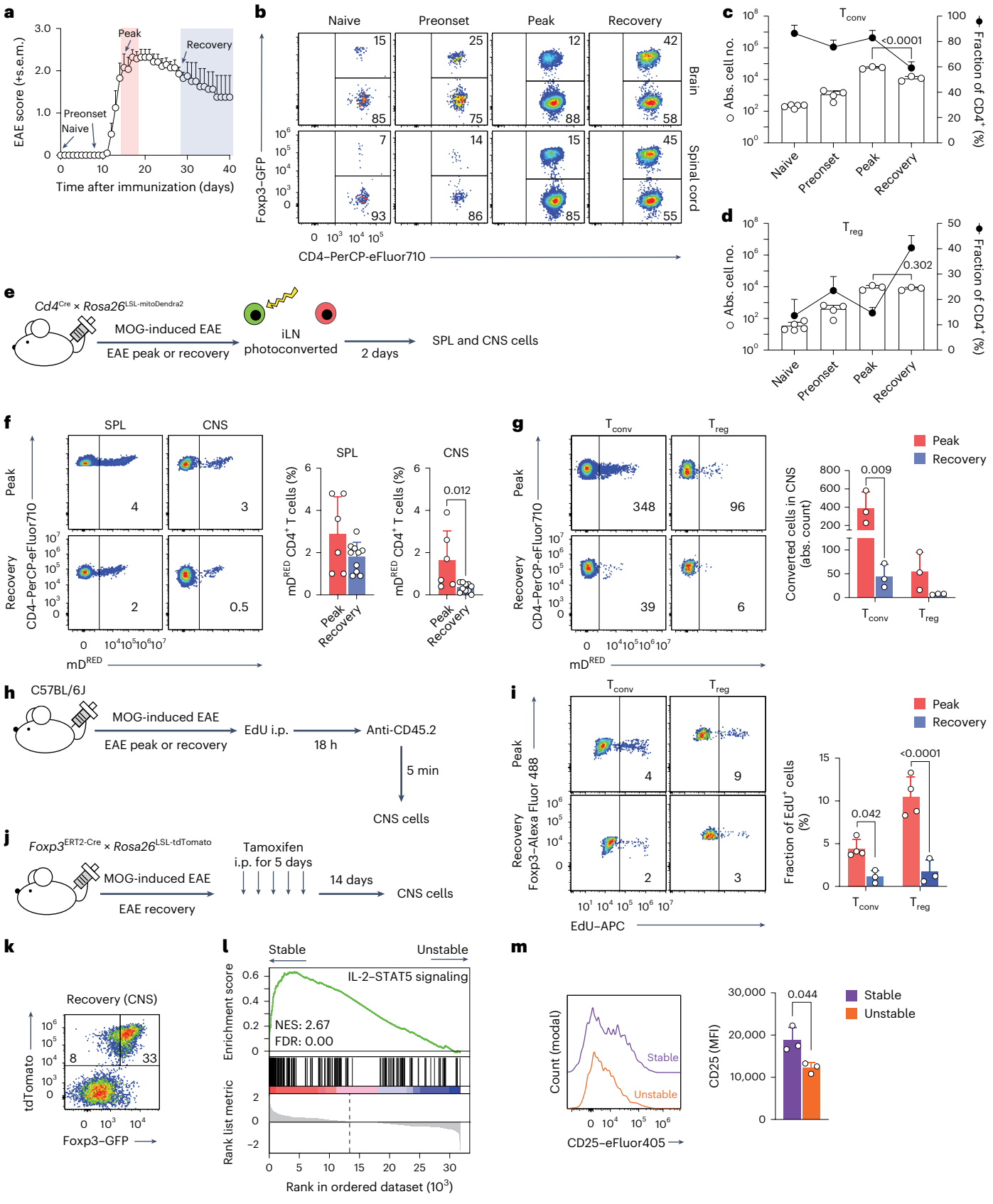

https://doi.org/10.1038/s41590-025-02416-z

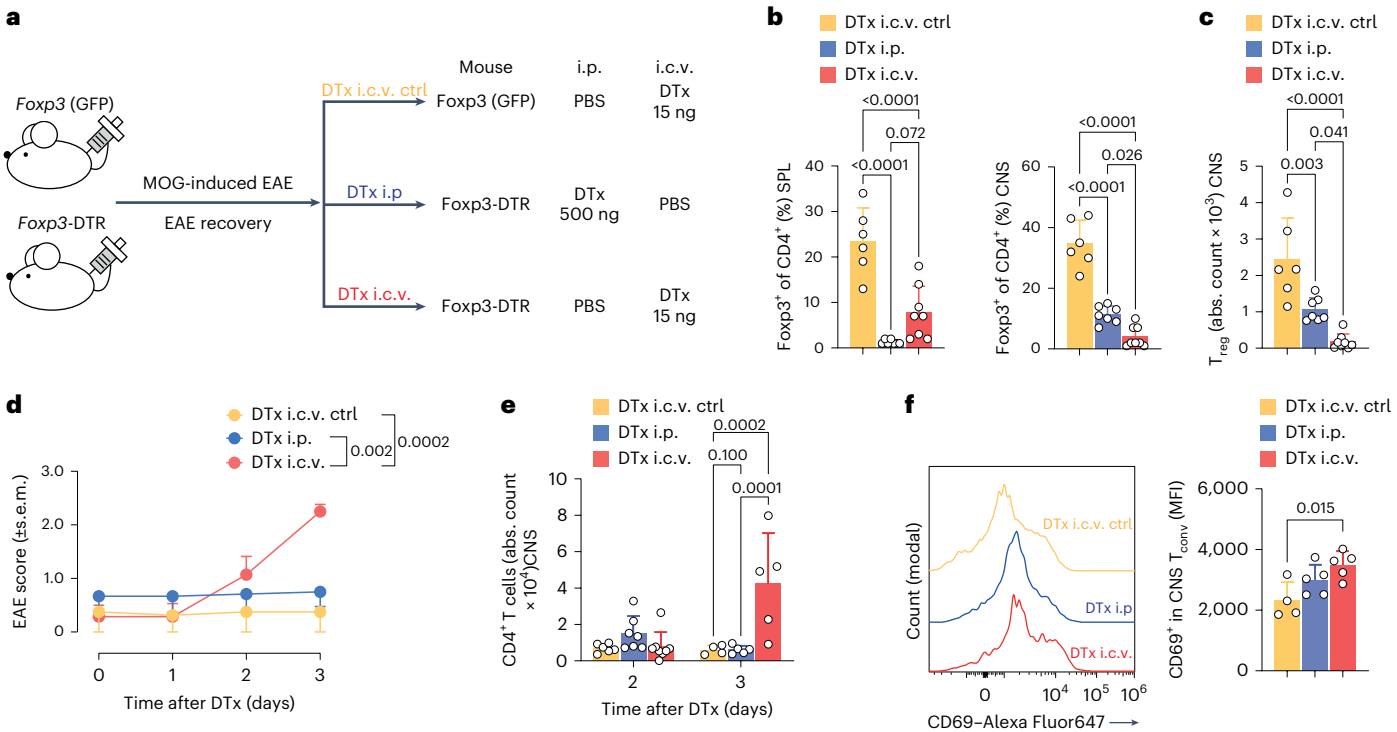

Fig. 2 | T_{reg} cells maintain immune homeostasis in the postinflammatory CNS. **a**, EAE was induced in *Foxp3* (GFP) and *Foxp3*-DTR mice. DTx was administered i.c.v. (15 ng) or i.p. (500 ng) during the recovery phase of EAE. Mice were killed 2 and 3 days after DTx injection, and spleen and CNS cells were isolated and analyzed by flow cytometry. **b**,**c**, The efficiency of T_{reg} cell depletion 2 days after DTx injection is shown in the spleen and CNS by the T_{reg} cell percentage (**b**) and the CNS T_{reg} cell count (**c**). Each symbol in **b** and **c** represents an individual mouse. Data are shown as mean + s.d. *P* values were calculated using a one-way ANOVA with a Tukey's HSD test (DTx i.c.v. control $n = 6$, DTx i.p. $n = 7$, DTx i.c.v. $n = 8$). **d**, EAE scores after DTx administration are shown as mean + s.e.m. (only including scores of mice followed up until the day 3 endpoint). *P* values were calculated using a two-way ANOVA with a Tukey's post hoc test (DTx i.c.v. control $n = 4$, DTx i.p. $n = 5$, DTx i.c.v. $n = 7$ biological replicates). **e**, $CD4^+$ T cell counts in the CNS at different time points after DTx administration. Each symbol represents an individual mouse. Data are shown as mean + s.d. *P* values were calculated using a two-way ANOVA with a Tukey's HSD test (day 2: DTx i.c.v. control $n = 6$, DTx i.p. $n = 7$, DTx i.c.v. $n = 8$; day 3: DTx i.c.v. control $n = 4$, DTx i.p. $n = 5$, DTx i.c.v. $n = 5$ biological replicates). **f**, CD69 expression (MFI) on CNS $CD4^+$ T_{conv} cells on day 3 after DTx treatment. Symbols represent individual mice. Data are shown as mean + s.d. *P* values were calculated using a one-way ANOVA with a Tukey's HSD test (DTx i.c.v. control $n = 4$, DTx i.p. $n = 5$, DTx i.c.v. $n = 5$ biological replicates).

Stress-tolerant T_{reg} cells control compartmentalized CNS inflammation

To study the functional relevance of CNS-residing stress-tolerant T_{reg} cells after resolution of acute inflammation (>day 35), we used *Foxp3*-DTR mice, which harbor a knock-in of the diphtheria toxin (DTx) receptor (DTR) gene expressed under the control of the endogenous *Foxp3* locus, for transient ablation of Foxp3-expressing cells via administration of DTx[27]. Because a complete depletion of T_{reg} cells from the CNS at late stages of EAE is challenging to achieve using the conventional systemic (intraperitoneal (i.p.) or intravenous (i.v.)) routes of DTx injection, we chose to administer low doses of DTx (15 ng) directly into the CNS using stereotactic intracerebroventricular (i.c.v.) injection (Fig. 2a). Local DTx delivery resulted in almost complete removal of CNS T_{reg} cells, while the systemic compartment was only transiently (and partially) depleted of $Foxp3^+$ T_{reg} cells (Fig. 2b,c). Depletion of CNS T_{reg} cells was accompanied by a rapid worsening of EAE symptoms (Fig. 2d and Extended Data Fig. 3), that is, the return of complete hind limb paralysis. Although some relapses were controlled again after 5 days, most DTx-treated mice succumbed to their relapses (Extended Data Fig. 3b,c). The disease relapses of i.c.v. DTx-injected *Foxp3*-DTR mice were not due to DTx-mediated CNS toxicity because i.c.v. DTx-injected wild-type control mice did not show any exacerbation of clinical symptoms. By contrast, efficient systemic depletion of T_{reg} cells in recovered EAE mice by i.p. DTx injection, which largely spared the CNS T_{reg} cell compartment, failed to trigger an EAE relapse (Fig. 2d).

Only the near-complete (i.c.v. DTx), but not the partial (i.p. DTx), depletion of CNS T_{reg} cells led to a marked increase in the amount of activated $CD4^+CD69^+$ T cells in the CNS of *Foxp3*-DTR mice by day 3 after DTx administration (Fig. 2e,f). In histologic analyses, T cells and myeloid cells primarily expanded at the sites of pre-existing inflammatory infiltrates after i.c.v. injection of DTx into post-EAE *Foxp3*-DTR mice (Fig. 3a,b). Although some effector cells were recruited from the systemic compartment (Fig. 3c), FTY720 did not prevent the massive activation of those T_{conv} cells already residing in the CNS (Fig. 3d). Their activation status was similar to the activation of CNS T_{conv} cells in non-FTY720-treated i.c.v. DTx-injected mice (Fig. 3d). Accordingly, FTY720 treatment failed to prevent EAE relapse following complete local depletion of recovery CNS T_{reg} cells (Fig. 3e), suggesting that residual CNS T_{conv} cells are sufficient to drive a relapse following removal of local T_{reg} cells.

In summary, stress-tolerant CNS T_{reg} cells, but not systemic T_{reg} cells, are essential for maintaining immune homeostasis in postinflammatory EAE mice.

Stress-tolerant CNS T_{reg} cells have a tissue-type transcriptome

To determine whether the changing inflammatory milieu within the CNS between the peak and the remission phase of EAE would shape the transcriptional profile of stress-tolerant CNS T_{reg} cells, we performed RNA-seq of bulk $CD4^+Foxp3\,(GFP)^+$ T_{reg} cells and $CD4^+Foxp3\,(GFP)^-$ T_{conv} cells sorted by fluorescence-activated cell sorting (FACS) from the spleen and CNS on days 15 and 40 after EAE induction.

https://doi.org/10.1038/s41590-025-02416-z

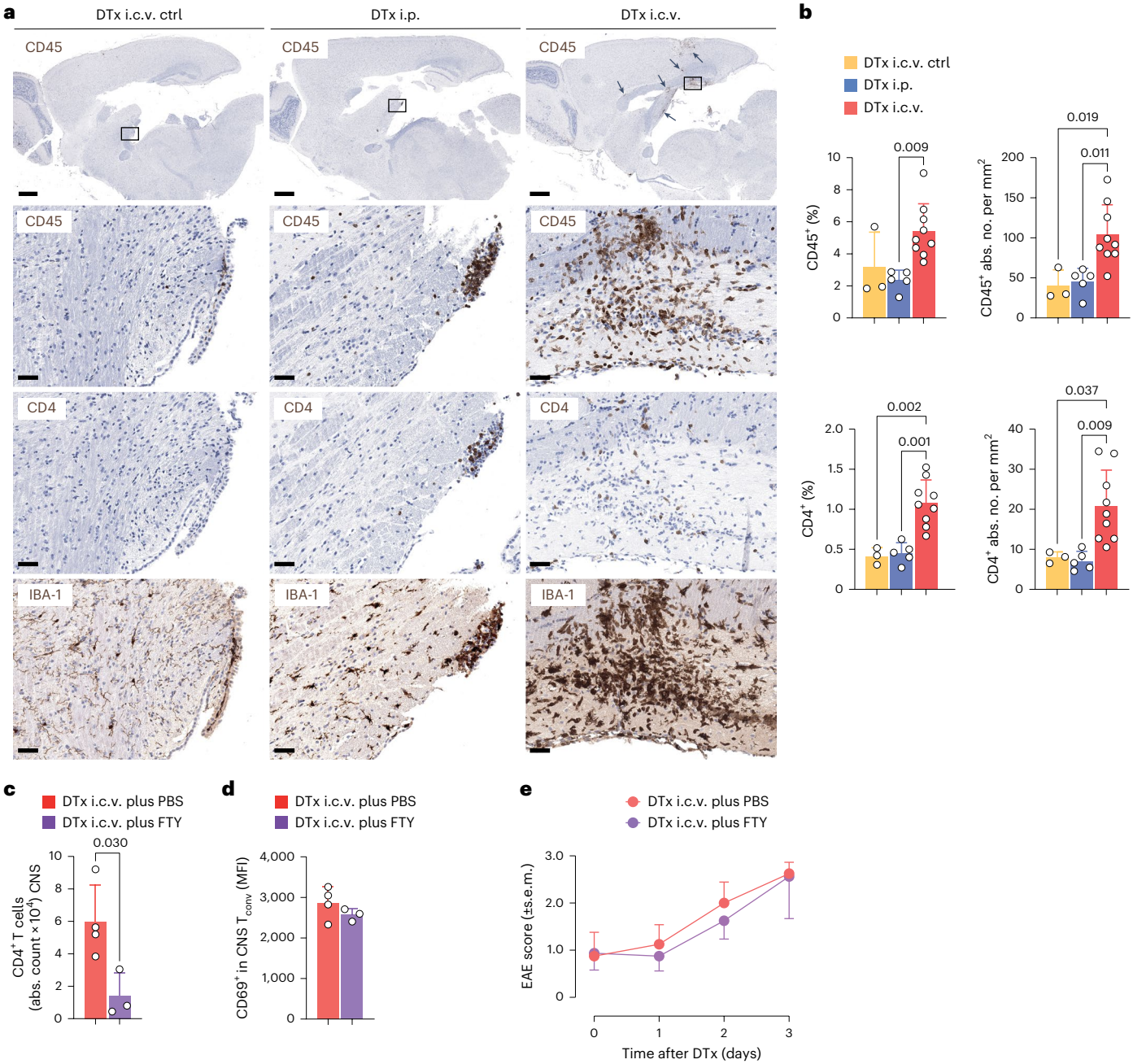

Fig. 3 | Loss of T_{reg} cells in the postinflammatory CNS rekindles inflammation. **a**, EAE was induced in *Foxp3* (GFP) and *Foxp3*-DTR mice. DTx was administered i.c.v. or i.p. during the recovery phase of EAE. Mice were killed 3 days after DTx injection. Brains were collected for immunohistochemistry staining. Arrows and squares indicate immune cell niches. Representative stainings for CD45, CD4 and IBA-1 are shown; scale bars, top row: 800 µm, bottom three rows: 50 µm. **b**, Quantification of $CD45^+$ and $CD4^+$ cells as percentages and absolute counts per mm^2. Symbols represent individual mice. Data are shown as mean + s.d. *P* values were calculated using a one-way ANOVA with a Tukey's HSD test (DTx i.c.v. control $n = 3$, DTx i.p. $n = 5$, DTx i.c.v. $n = 9$ biological replicates). **c**,**d**, EAE was induced in *Foxp3*-DTR mice, and DTx was administered i.c.v. during the recovery phase. FTY720 (FTY; 1 µg per gram per day) or PBS was administered i.p. from 24 h before to 72 h after DTx i.c.v. injection. $CD4^+$ T cell counts in the CNS (**c**) and MFI of CD69 on CNS $CD4^+$ T_{conv} cells (**d**) as determined by flow cytometry are shown. Symbols represent individual mice. Data are shown as mean + s.d. The *P* value in **c** was determined by a two-tailed unpaired Student's *t*-test (DTx i.c.v. plus PBS $n = 4$, DTx i.c.v. plus FTY $n = 3$ biological replicates). **e**, EAE scores after i.c.v. DTx administration shown as mean + s.e.m. (DTx i.c.v. plus PBS $n = 4$, DTx i.c.v. plus FTY $n = 4$ biological replicates).

RNA-seq analysis revealed a total of 311 differentially expressed genes (DEGs; >1.5-fold, adjusted $P < 0.05$) between CNS T_{reg} cells derived from EAE recovery and EAE peak, with 159 genes upregulated in recovery CNS T_{reg} cells and 152 genes upregulated in peak CNS T_{reg} cells (Extended Data Fig. 4a), consistent with a distinct positioning of CNS T_{reg} cells along principal component 2 (PC2) according to the disease phase (Fig. 4a). The number of disease-phase conditional DEGs was smaller within splenic T_{reg} cells, with only 15 upregulated and 6 downregulated genes in recovery splenic T_{reg} cells versus peak splenic T_{reg} cells. Compared to their disease-phase-specific splenic counterparts, both recovery and peak CNS T_{reg} cells showed an upregulation of several genes that have previously been associated with a nonlymphoid tissue T_{reg} cell phenotype, including *Areg*, *Nfil3*, *Prdm1*, *Rora*, *Itgae*, *Icos*, *Il10*, *Il1rl1* and *Il2ra* (Extended Data Fig. 4b,c). Although most of the tissue

T_{reg} cell-associated genes did not undergo disease-phase-dependent changes in expression, the 'TNF signaling via NF-κB' and 'IL-2–STAT5 signaling' pathways were the two top upregulated pathways in recovery CNS T_{reg} cells compared to peak CNS T_{reg} cells (Extended Data Fig. 4a–h), suggesting that the optimal exploitation of limited amounts of IL-2 after the contraction of the IL-2-producing effector T cell population (see Fig. 1c) might become the most crucial determinant of their 'resilience to stress' in CNS recovery T_{reg} cells.

To identify upstream and downstream determinants of the stress-tolerant CNS T_{reg} cell functional phenotype, we first analyzed genes differentially expressed in recovery CNS versus peak CNS T_{reg} cells, which encoded cell surface proteins or DNA-binding proteins with transcription factor activity (Fig. 4b,c). We then performed functional enrichment analyses, only selecting those DEGs that were not at the same time significantly regulated in recovery versus peak T_{conv} cells to define a CNS T_{reg} cell-exclusive signature of up- and downregulated transcripts in the recovery phase (Fig. 4d and Supplementary Table 3). Functional enrichment analyses with the upregulated genes revealed a few significantly regulated cellular processes, including 'response to stress' (Fig. 4e). Notably, the genes that were exclusively upregulated in recovery CNS T_{reg} cells and at the same time intersected the GO terms 'response to stress' and 'cell surface' comprised *Nrp1*, *Cxcr6*, *Cxcr4*, *Sdc4*, *H2-Aa*, *H2-Ab*, *Lag3*, *Fasl* and *Cd38* (Fig. 4f). Those recovery CNS T_{reg} cell DEGs that intersected the GO terms 'response to stress' and 'transcription factor activity' comprised *Rbpj*, *Nr4a1*, *Nr4a2*, *Nfatc1*, *Klf10*, *Zeb2* and *Irf4* (Fig. 4g). Together, these data suggest that T cell antigen receptor (TCR) signaling and IL-2 signaling are defining features of the functional phenotype of stress-tolerant T_{reg} cells residing in the chronically inflamed CNS. Interestingly, CD38 was strongly linked to this T_{reg} cell phenotype.

Stress-tolerant T_{reg} cells and tissue T_{reg} cells share features

To test whether stress-tolerant T_{reg} cells in the postinflammatory CNS are distinct from bona fide tissue T_{reg} cells, we compared their transcriptome with the transcriptomes of T_{reg} cells isolated from the CNS of unmanipulated naive mice and prototypic tissue T_{reg} cells isolated from the visceral adipose tissue (VAT). Due to the scarcity of Foxp3$^+$ T_{reg} cells in the CNS of naive mice, the cell input had to be adjusted to a lower number in this RNA-seq analysis, resulting in a lower overall sequencing depth across all samples. Nevertheless, PC analysis of the 500 top most variable genes revealed a clear separation along PC1 of the transcriptome of CNS-derived T_{reg} cell populations from the transcriptome of steady-state VAT T_{reg} cells, in part driven by the considerably higher expression of tissue T_{reg}-associated genes such as *Areg*, *Klrg1*, *Gata3* and *Il1rl1* in VAT T_{reg} cells (Fig. 5a). However, stress-tolerant T_{reg} cells also showed a clear overlap with VAT T_{reg} cells for the expression of other tissue T_{reg}-associated genes (Extended Data Fig. 5a), suggesting that stress-tolerant T_{reg} cells adopt key features of bona fide tissue T_{reg} cells. Notably, within the CNS T_{reg} cell compartment, the transcriptome of stress-tolerant T_{reg} cells resembled that of naive CNS T_{reg} cells, and both separated along PC2 from the transcriptome of T_{reg} cells isolated during the peak of disease (Fig. 5a), indicating that the stress-tolerant CNS T_{reg} cell transcriptional profile reverts back to a more steady-state-like gene expression. However, despite the similarities to the transcriptome of homeostatic CNS T_{reg} cells, gene set enrichment analysis (GSEA) again confirmed an enrichment in the IL-2 signaling pathway in stress-tolerant CNS T_{reg} cells versus naive CNS T_{reg} cells (Fig. 5b and Extended Data Fig. 5b–d), whereas naive CNS T_{reg} cells were characterized by more prominent oxidative phosphorylation than stress-tolerant postinflammatory CNS T_{reg} cells (Fig. 5c and Extended Data Fig. 5b–d). A selection of T_{reg} cell-associated surface markers, including CD69, CXCR4 and CD38, was markedly expressed in stress-tolerant CNS T_{reg} cells and to a lesser extent in naive CNS T_{reg} cells, whereas KLRG1 and ST2 were highly upregulated in VAT T_{reg} cells (Fig. 5d,e). Together, these data indicate that postinflammatory stress-tolerant CNS T_{reg} cells adopt a CNS-specific tissue signature[28] with a particular dependence on IL-2.

Lack of CD38 impairs the regulatory capacity of CNS Foxp3$^+$ T_{reg} cells

CD38 was upregulated in T_{reg} cells in the inflamed CNS, whereas we did not observe disease-phase-dependent upregulation of CD38 in T_{conv} cells (Fig. 6a). CD38 is the major NAD^+ hydrolyzing ectoenzyme[29]. In fact, CD38 is indispensable for maintaining the concentration of NAD^+ in the microenvironment at low levels. High levels of NAD^+, in turn, drive the ADP-ribosylation of cell surface molecules by ADP-ribosyltransferase 2b (ARTC2.2), a toxin-related, GPI-anchored ADP-ribosyltransferase expressed in T cells. ARTC2.2 has multiple target molecules that can gain or lose activity through ADP-ribosylation[30].

To test whether CD38 expression by T_{reg} cells is relevant in autoimmune CNS inflammation, we developed an experimental model in which we adoptively transferred T_{reg} cell populations enriched for MOG-reactive T_{reg} cells that were either sufficient or deficient in CD38 into MOG-immunized host mice whose T_{reg} cell compartment was acutely depleted immediately before T_{reg} cell transfer (Fig. 6b). The transfer of MOG-activated wild-type T_{reg} cells attenuated the EAE severity of recipient mice compared to control EAE mice that were T_{reg} cell depleted but did not receive a subsequent T_{reg} cell transfer (Fig. 6c). By contrast, the adoptive transfer of MOG-activated CD38-deficient T_{reg} cells failed to control EAE symptoms of recipient mice that became as sick as control animals without transfer of T_{reg} cells (Fig. 6c), suggesting that *Cd38*$^{-/-}$ T_{reg} cells had a T_{reg} cell-intrinsic deficiency to regulate EAE. Because CD38-deficient T_{reg} cells were equally recruited to the CNS as wild-type T_{reg} cells (Fig. 6d–f), we speculated that CD38 was directly or indirectly involved in the formation and maintenance of a productive effector T_{reg} cell population in the CNS.

To gauge the particular significance of CD38 expression for the functional phenotype of stress-tolerant postinflammatory T_{reg} cells in nonlymphoid tissues (especially in the CNS), we generated a

Fig. 4 | Transcriptome analysis of CNS T_{reg} cells during different phases of EAE. EAE was induced in *Foxp3* (GFP) reporter mice. T_{conv} and T_{reg} cells were sorted from the spleen and CNS during peak EAE or the recovery phase (rec) and were subjected to bulk RNA-seq. **a**, PC analysis. Each symbol represents an individual mouse. **b**,**c**, Volcano plots showing genes with annotation to the Gene Ontology (GO) terms 'GO:0009986 cell surface' (**b**) and 'GO:0003700 DNA binding transcription factor activity' (**c**) with differential expression (≥1.5-fold, adjusted $P < 0.05$) between recovery phase and peak CNS T_{reg} cells. DEGs are highlighted in orange. Adjusted *P* values were derived from DESeq2 using a two-tailed Wald's test with correction for multiple testing using the Benjamini and Hochberg method (CNS T_{reg} peak $n = 4$, CNS T_{reg} recovery phase $n = 5$ biological replicates); TF, transcription factor. **d**, Heat map with hierarchical clustering of DEGs between CNS recovery phase and peak T_{reg} cells. DEGs with the same phase-dependent regulation in CNS T_{conv} cells as in CNS T_{reg} cells were subtracted to yield a CNS T_{reg} private gene signature. **e**, Upregulated DEGs from the recovery phase CNS T_{reg} private signature were used to perform GO enrichment analysis (gprofiler 2g:GOSt). *P* values are derived from Fisher's one-tailed test, and adjusted *P* values were determined by the g:GOSt implemented g:SCS method for multiple testing correction. The top five enriched terms are marked and summarized in the table on the right; MF, molecular function; CC, cellular component; BP, biological process; KEGG, Kyoto Encyclopedia of Genes and Genomes; REAC, Reactome; WP, WikiPathways; Reg., regulation; multicell., multicellular; org., organismal; proc., process; Pos., positive; biol., biological. **f**,**g**, Volcano plots displaying only genes that are part of both the GO terms 'response to stress' (GO:0006950) and 'cell surface' (GO:0009986; **f**) or 'DNA-binding transcription factor activity' (GO:0003700; **g**) between CNS recovery phase and peak T_{reg} cells. DEGs (≥1.5-fold, adjusted $P < 0.05$) from the recovery phase CNS T_{reg} private 'up' signature are highlighted in purple. Adjusted *P* values are derived from DESeq2 using a two-tailed Wald's test with correction for multiple testing using the Benjamini and Hochberg method.

https://doi.org/10.1038/s41590-025-02416-z

mixed bone marrow chimera (MBMC) model by transplanting a 1:1 mixture of wild-type *Foxp3*-DTR^{+} (CD45.1/CD45.2) and 'nondepletable' *Foxp3*-DTR^{-} (CD45.2) donor cells of either wild-type or *Cd38*$^{-/-}$ origin into *Rag1*$^{-/-}$ recipient mice (Fig. 6g). CNS-specific depletion of DTR-expressing wild-type T_{reg} cells in these MBMCs by local DTx injection during stable post-peak EAE allowed us to follow disease progression in a scenario in which the remaining CNS-residing T_{reg} cells were either wild-type or CD38 deficient (Fig. 6g–i). Notably, the T_{conv}

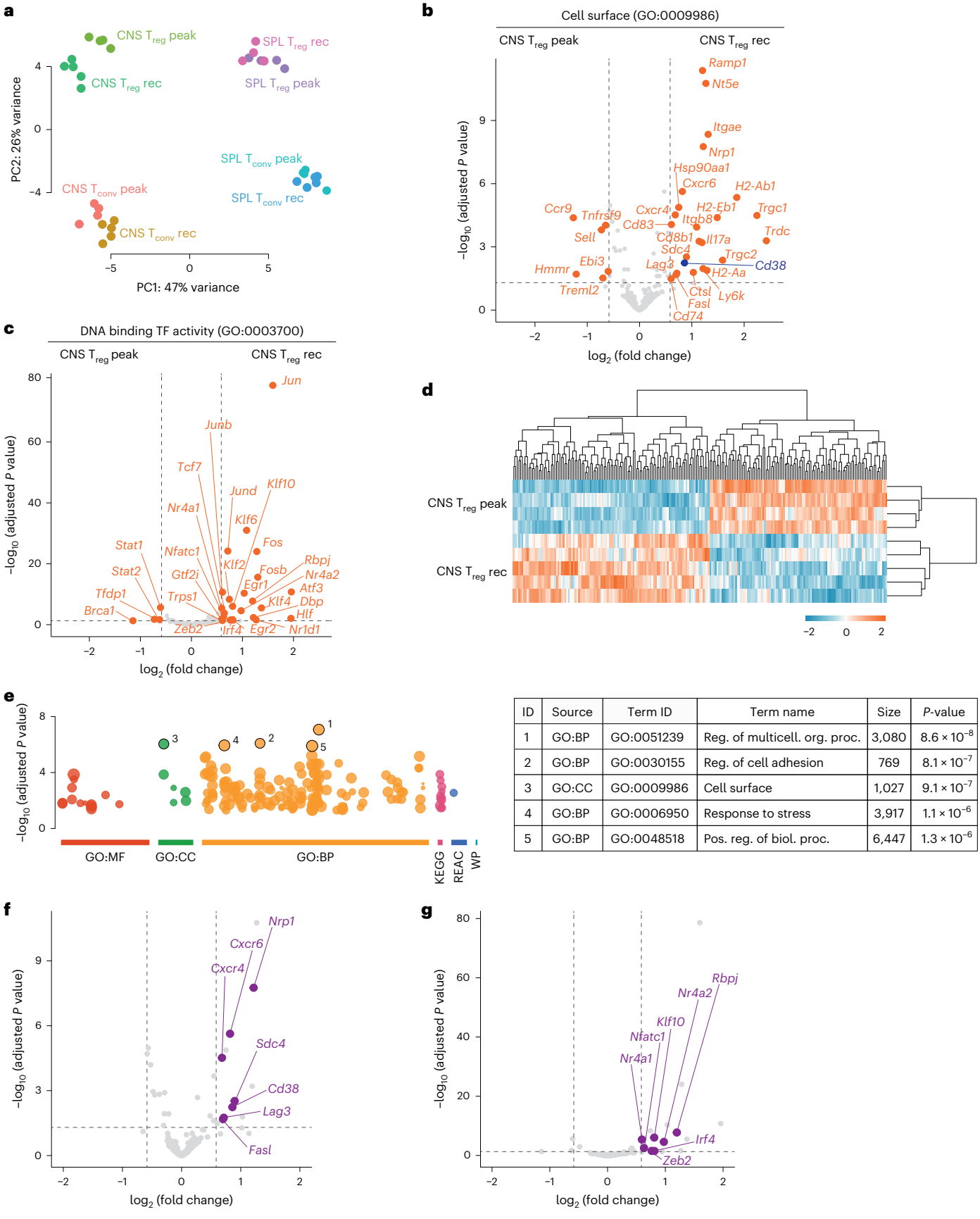

ID	Source	Term ID	Term name	Size	*P*-value
1	GO:BP	GO:0051239	Reg. of multicell. org. proc.	3,080	8.6×10^{-8}
2	GO:BP	GO:0030155	Reg. of cell adhesion	769	8.1×10^{-7}
3	GO:CC	GO:0009986	Cell surface	1,027	9.1×10^{-7}
4	GO:BP	GO:0006950	Response to stress	3,917	1.1×10^{-6}
5	GO:BP	GO:0048518	Pos. reg. of biol. proc.	6,447	1.3×10^{-6}

https://doi.org/10.1038/s41590-025-02416-z

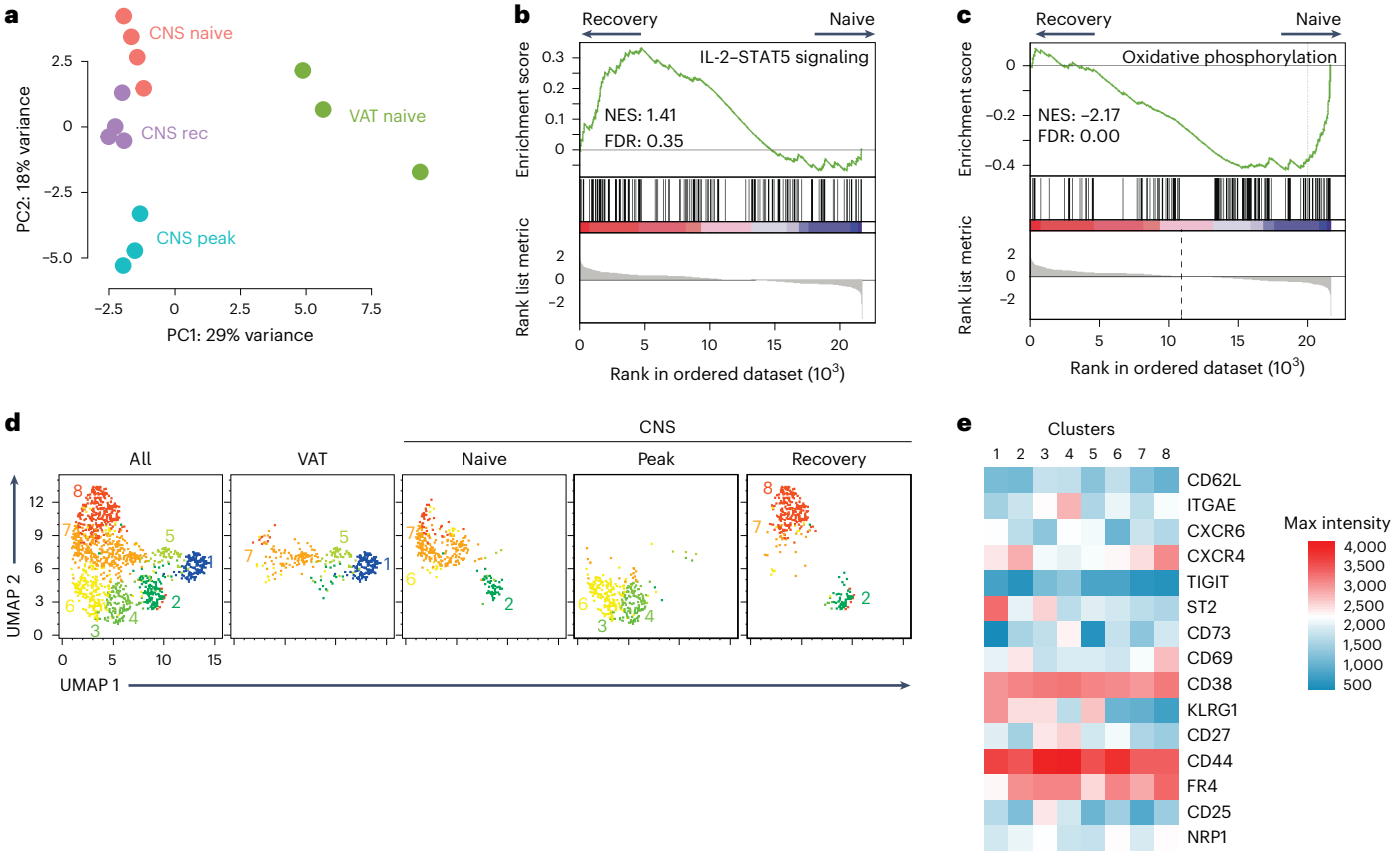

Fig. 5 | Recovery CNS T_{reg} cells resemble steady-state CNS T_{reg} cells. *Foxp3* (GFP)$^+$ T_{reg} cells were isolated from VAT and the CNS of naive mice and EAE mice at the peak ($n = 3$) and recovery stages and were subjected to bulk RNA-seq (VAT naive $n = 3$, CNS naive $n = 4$, CNS peak $n = 3$, CNS recovery $n = 4$ biological replicates). **a**, PC analysis. **b**,**c**, Enrichment plots for 'IL-2–STAT5 signaling' (**b**) and 'Oxidative phosphorylation' (**c**) derived from GSEAs comparing CNS recovery and CNS naive T_{reg} cells. **d**, CD4$^+$Foxp3$^+$ T_{reg} cells from the naive CNS, VAT and the EAE CNS (peak and recovery) were analyzed by flow cytometry. Flow data were pooled (CNS naive $n = 3$, CNS peak $n = 4$, CNS recovery $n = 3$, VAT naive $n = 3$ biological replicates) and downsampled to 300 T_{reg} cells per group. T_{reg} cells were clustered by FlowSOM and visualized using uniform manifold approximation and projection (UMAP). **e**, Heat map displaying marker expression in T_{reg} cell metaclusters.

cell compartment was composed of either only wild-type cells (*Cd38*$^{+/+}$ MBMC) or a 1:1 mixture of wild-type and *Cd38*$^{-/-}$ T cells (*Cd38*$^{-/-}$ MBMCs; Fig. 6h). Consistent with our observation that the severity of EAE was reduced in a gene dose-dependent manner in globally CD38-deficient mice (Extended Data Fig. 6a), *Cd38*$^{-/-}$ MBMCs experienced a milder disease course than *Cd38*$^{+/+}$ MBMCs (Extended Data Fig. 6b). Nevertheless, following local depletion of *Foxp3*-DTR T_{reg} cells, the remaining nondepletable wild-type T_{reg} cells in *Cd38*$^{+/+}$ MBMCs were sufficient to maintain a stable EAE score (Fig. 6j and Extended Data Fig. 6b), even when faced with a fully CD38-competent CNS-resident T_{conv} cell compartment. By contrast, *Cd38*$^{-/-}$ MBMCs, with only *Cd38*$^{-/-}$ CNS T_{reg} cells remaining after local depletion of the wild-type T_{reg} cell fraction, rapidly deteriorated and experienced an EAE relapse with similar kinetics and intensity as we had observed after the complete depletion of CNS T_{reg} cells (Fig. 6j and Extended Data Fig. 6b; see also Fig. 2d). These data highlight that cell-autonomous expression of CD38 in CNS-resident T_{reg} cells is indispensable for adequate control of local immune homeostasis in the chronically inflamed CNS in vivo.

CD38 is crucial for maintenance of antigen-specific CNS T_{reg} cells

Foxp3$^+$ T_{reg} cells need to be activated in an antigen-specific manner to efficiently control effector T cells in EAE[31]. Therefore, the most direct link to the failure of CD38-deficient T_{reg} cells to control EAE would be the lack of MOG-specific T_{reg} cells within the population of *Cd38*$^{-/-}$ CNS T_{reg} cells. Indeed, in the CNS, $MOG_{35–55}$–I-Ab tetramer-binding T_{reg} cells were virtually entirely comprised in the CD38$^+$ compartment, remarkably during EAE recovery (Fig. 7a–c).

To test whether CD38 status determined the fraction of MOG-specific T_{conv} and T_{reg} cells, we induced EAE in MBMCs, whose hematopoietic compartment consisted of wild-type (CD45.1) and *Cd38*$^{-/-}$ (CD45.2) cells, and read out the fraction of $MOG_{35–55}$–I-Ab-binding cells in T_{conv} and T_{reg} cells in each cellular compartment that were present side-by-side in the same chronically inflamed CNS (day 20 after immunization; Fig. 7d). Notably, although CD38 expression was irrelevant for the fraction of MOG-specific T_{conv} cells in the CNS, the fraction of MOG-specific CNS T_{reg} cells was significantly lower in CD38-deficient cells than in CD38-sufficient T cells (Fig. 7e,f). Together, these data indicate that the presence of antigen-specific Foxp3$^+$ T_{reg} cells, but not antigen-specific T_{conv} cells, in the inflamed CNS is dependent on the cell-intrinsic expression of CD38. This may be particularly relevant for high-affinity antigen-specific T_{reg} cells because MOG–I-Ab tetramer staining identifies high-affinity MOG-specific T_{reg} cells[32].

Stress-tolerant CNS T_{reg} cells are dependent on CD38 for sensing IL-2

To dissect the mechanism by which CD38 contributes to the maintenance of antigen-specific T_{reg} cells in the postinflammatory CNS, we referred to its known function as an NAD$^+$-consuming enzyme and speculated that T_{reg} cells might be more susceptible to NAD$^+$-induced

cell death than T_{conv} cells in the chronically inflamed CNS. To directly test this hypothesis, we induced EAE in *Foxp3* (GFP) reporter mice and, in the recovery stage, challenged the mice by i.c.v. injection of NAD^+ in the absence or presence of an inhibitor of ARTC2.2 (Fig. 8a). Although NAD^+ injection directly resulted in the apoptosis of around 90% of all CNS T_{reg} cells, CNS T_{conv} cells were spared from apoptosis (Fig. 8b–d). Interestingly, i.c.v. injection of NAD^+ did not affect T_{reg} cells or T_{conv} cells in the systemic immune compartment (Extended Data Fig. 7a–c). In the CNS of recovery EAE mice, NAD^+-induced apoptosis was entirely rescued by the co-injection of a blocking nanobody to ARTC2.2 together with NAD^+ (Fig. 8b–d), suggesting that ADP-ribosylation by ARTC2.2 was the key downstream mediator of NAD^+-induced cell death in vivo. Also, these data were consistent with an in vivo effect of NAD^+ and not an artificial release of NAD^+ from cells during the preparation procedure[33]. Although the gain-of-function of $P2RX_7$ through ADP-ribosylation has previously been shown to drive cell death[23], the expression of $P2RX_7$ was not different between T_{reg} cells and T_{conv} cells in the postinflammatory CNS. Yet, T_{conv} cells were relatively resistant to NAD^+-induced apoptosis, whereas T_{reg} cells were not. Therefore, we explored alternative T_{reg} cell-specific ADP-ribosylation targets. Because IL-2 signaling had turned out to be a major determinant of stress-tolerant CNS T_{reg} cells, we first focused on the IL-2Rα subunit, which is highly expressed in antigen-specific T_{reg} cells (Extended Data Fig. 8a–c). Here, we made use of the prior observation that the R178 ADP-ribosylated hypofunctional form of IL-2Rα is not recognized by the 7D4 clone of anti-CD25, whereas the PC61.5 clone of anti-CD25 detects both the native and the ADP-ribosylated form of IL-2Rα[34]. To investigate IL-2Rα ADP-ribosylation status, wild-type or CD38-deficient T_{reg} cells were exposed to NAD^+ in vitro in the absence or presence of ARTC2.2-inhibiting nanobodies. Although IL-2Rα was mostly not ADP-ribosylated in wild-type T_{reg} cells, 80% of IL-2Rα was ADP-ribosylated in CD38-deficient T_{reg} cells. Notably, wild-type T_{reg} cells were essentially resistant to further ADP-ribosylation induced by NAD^+ exposure. By contrast, IL-2Rα became fully ADP-ribosylated through NAD^+ in CD38-deficient T_{reg} cells, a process that was prevented by a blocking nanobody to ARTC2.2 (Fig. 8e,f). In line with the idea that ADP-ribosylation of IL-2Rα leads to deficient IL-2 signaling through the high-affinity IL-2R expressed in T_{reg} cells (Fig. 8g), NAD^+ exposure reduced STAT5 phosphorylation significantly more in CD38-deficient T_{reg} cells than in wild-type T_{reg} cells in an ARTC2.2-dependent manner (Fig. 8h,i). Finally, IL-2Rα ADP-ribosylation was significantly more pronounced in CD38-deficient T_{reg} cells than in their wild-type counterparts, even when T_{reg} cells of both genotypes were cocultured together in the same dish during NAD^+ exposure (Fig. 8j), suggesting that cell-intrinsic expression of CD38 was crucial to achieve low levels of NAD^+ in the proximal vicinity of the cell and, thus, prevent ADP-ribosylation of its surface molecules. Together, these data illustrate that T_{reg} cell-autonomous expression of CD38 is essential for their perception of restricted amounts of IL-2, as would occur in 'stressful' nonlymphoid environments.

Discussion

In the present study, we show that $Foxp3^+$ T_{reg} cells persist in the CNS for extended periods of time after the contraction of pathogenic effector T cells. These CNS-resident T_{reg} cells are indispensable for maintaining the re-established immune homeostasis in the CNS after an autoimmune inflammatory episode, as their site-specific depletion immediately triggers a relapse. The long-term persistence of T_{reg} cells in the postinflammatory CNS is dependent on the efficient exploitation of limited amounts of IL-2, which selects for antigen-specific T_{reg} cells with high expression of the high-affinity IL-2R CD25. These stress-tolerant T_{reg} cells, at the same time, must express CD38 to cope with enhanced levels of extracellular NAD^+, which otherwise dampen T_{reg} cell-intrinsic IL-2 signaling due to ADP-ribosylation of IL-2Rα. Therefore, the expression of the NAD^+ hydrolase CD38 critically determines the resilience of CNS T_{reg} cells to the hostile environment of the postinflammatory CNS and, thus, is a hallmark feature of stress-tolerant T_{reg} cells.

CD38 is a multifunctional molecule with diverse roles in various cellular processes. It acts as an NAD^+ consuming enzyme, thereby regulating both intracellular and extracellular NAD^+ levels[35,36]. Additionally, CD38 functions as a receptor of PECAM-1 (CD31), influencing leukocyte migration[37]. Although PECAM-1/CD38 interactions might affect T_{reg} cell migration into nonlymphoid tissues, our data indicate that T_{reg} cells can migrate to the inflamed CNS without CD38. $CD38^+$ T_{reg} cells possess a survival advantage in nonlymphoid tissues. Conversely, CD38-deficient T_{reg} cells fail to reduce extracellular NAD^+ concentrations in their micromilieu and, as a consequence, are more susceptible to ARTC2.2/$P2X_7$-mediated apoptosis, which is dependent on extensive Ca^{2+} influx through the ATP-gated $P2X_7$ receptor ion channel due to ARTC2.2-mediated ADP-ribosylation of $P2RX_7$ (refs. 38–40). However, although $P2RX_7$ is similarly expressed in T_{conv} and T_{reg} cells, the exaggerated susceptibility of T_{reg} (but not T_{conv}) cells to NAD^+-induced cell death in the CNS is likely due to further targets of ADP-ribosylation[30], such as IL-2Rα, which is orders of magnitude more highly expressed in T_{reg} cells than in T_{conv} cells. Here, ARTC2.2-mediated ADP-ribosylation leads to a loss-of-function of high-affinity IL-2Rα with reduced STAT5 activation. CD38 quenches ADP-ribosylation of IL-2Rα through removing membrane-proximal extracellular NAD^+ (in a cell-autonomous manner) as a substrate of ARTC2.2. Additionally, CD38 also competes for intracellular NAD^+, thereby influencing intracellular NAD^+-dependent pathways. Intracellular NAD^+ is an essential cofactor for sirtuins, which act as deacetylases of histones and, thus, play a role in gene silencing. Intracellular NAD^+ is also a cofactor for poly(ADP-ribosyl) polymerases, which are involved in DNA damage repair. These functions of NAD^+-dependent enzymes have been linked to cellular aging[41]. In the context of T cells, SIRT1 has been demonstrated to negatively regulate

Fig. 6 | CD38 signaling controls the functional phenotype of CNS T_{reg} cells. a, EAE was induced in *Foxp3* (GFP) mice, and CNS cells were collected and analyzed by flow cytometry to assess CD38 expression on T_{conv} ($CD4^+Foxp3^-$) and T_{reg} cells ($CD4^+Foxp3^+$) across EAE stages. Symbols represent individual mice. Data are shown as mean + s.d. *P* values were calculated using a two-way ANOVA with a Tukey's HSD test (naive $n = 10$, peak $n = 10$, recovery $n = 6$ biological replicates). **b**, EAE was induced in recipient DEREG mice (CD45.1) and donor $Cd38^{+/+}$ or $Cd38^{-/-}$ mice (CD45.2). T_{reg} cells in recipient mice were depleted by i.p. DTx injection at days 9 and 10 after EAE induction. In total, 10^5 sorted splenic donor T_{reg} cells ($CD4^+CD25^+GITR^+CD45.2^+$) were transferred into $CD45.1^+$ DEREG recipients. T_{reg} protector S+16a nanobody was i.p. administered to donor mice 30 min before euthanasia; d.p.i., days post immunization. **c**, Mean EAE scores + s.e.m. of recipient mice. *P* values were determined using a two-way ANOVA with a Tukey's post hoc test (without T_{reg} cell transfer (wo) $n = 5$, $Cd38^{+/+}$ T_{reg} cell transfer $n = 4$, $Cd38^{-/-}$ T_{reg} cell transfer $n = 5$ biological replicates). **d**–**f**, Donor $CD4^+CD45.2^+$ cells were analyzed and quantified in recipient lymph nodes (**d** and **e**) and CNS tissue (**d** and **f**). Each symbol in **e** and **f** represents an individual mouse, and the data are shown as mean + s.d.; Transf., transfer. **g**, BM from *Foxp3*-DTR mice (CD45.1/CD45.2) mixed 1:1 with either wild-type $Cd38^{+/+}$ (CD45.2) or $Cd38^{-/-}$ BM (CD45.2) was transferred into sublethally irradiated $Rag1^{-/-}$ recipients, and EAE was induced in BM-reconstituted mice. DTx was administered i.c.v. (15 ng) in stable EAE mice on day 28 after MOG_{35-55} immunization, and CNS cells were collected 3 days after DTx i.c.v. injection. **h**, Proportions of T_{reg} cells ($TCR\beta^+CD4^+Foxp3^+$) were analyzed in the *Foxp3*-DTR compartment ($CD45.1^+$) and in the CD38-sufficient or CD38-deficient compartment ($CD45.2^+$) within the CNS of MBMCs. **i**, Fraction of $CD38^+$ cells among total CNS T_{reg} cells 3 days after DTx injection. Symbols represent individual mice. Data are shown as mean + s.d. *P* values were calculated using an unpaired two-tailed Student's *t*-test ($Cd38^{+/+}$ MBMCs $n = 4$, $Cd38^{-/-}$ MBMCs $n = 5$ biological replicates). **j**, Changes in EAE scores (ΔEAE scores) after DTx injection shown as mean + s.e.m. ($Cd38^{+/+}$ MBMCs $n = 4$, $Cd38^{-/-}$ MBMCs $n = 5$ biological replicates).

https://doi.org/10.1038/s41590-025-02416-z

T_{reg} cell function by decreasing the expression of Foxp3 and CTLA-4, while simultaneously increasing DNMT3a expression[42]. The absence of CD38 could lead to excess NAD^+ availability, which may enhance SIRT1 activity and dismantle T_{reg} cell stability. However, here, we did not observe a difference in Foxp3 expression in CD38-deficient T_{reg} cells compared to wild-type T_{reg} cells in the same environment. Furthermore, CD38 regulates intracellular Ca^{2+} levels via the cyclic adenosine 5′-diphosphate ribose (cADPR) signaling pathway, which may influence T cell differentiation[43]. Proper Ca^{2+} influx is critical for T_{reg} cell functionality, and impaired Ca^{2+} signaling has been associated with

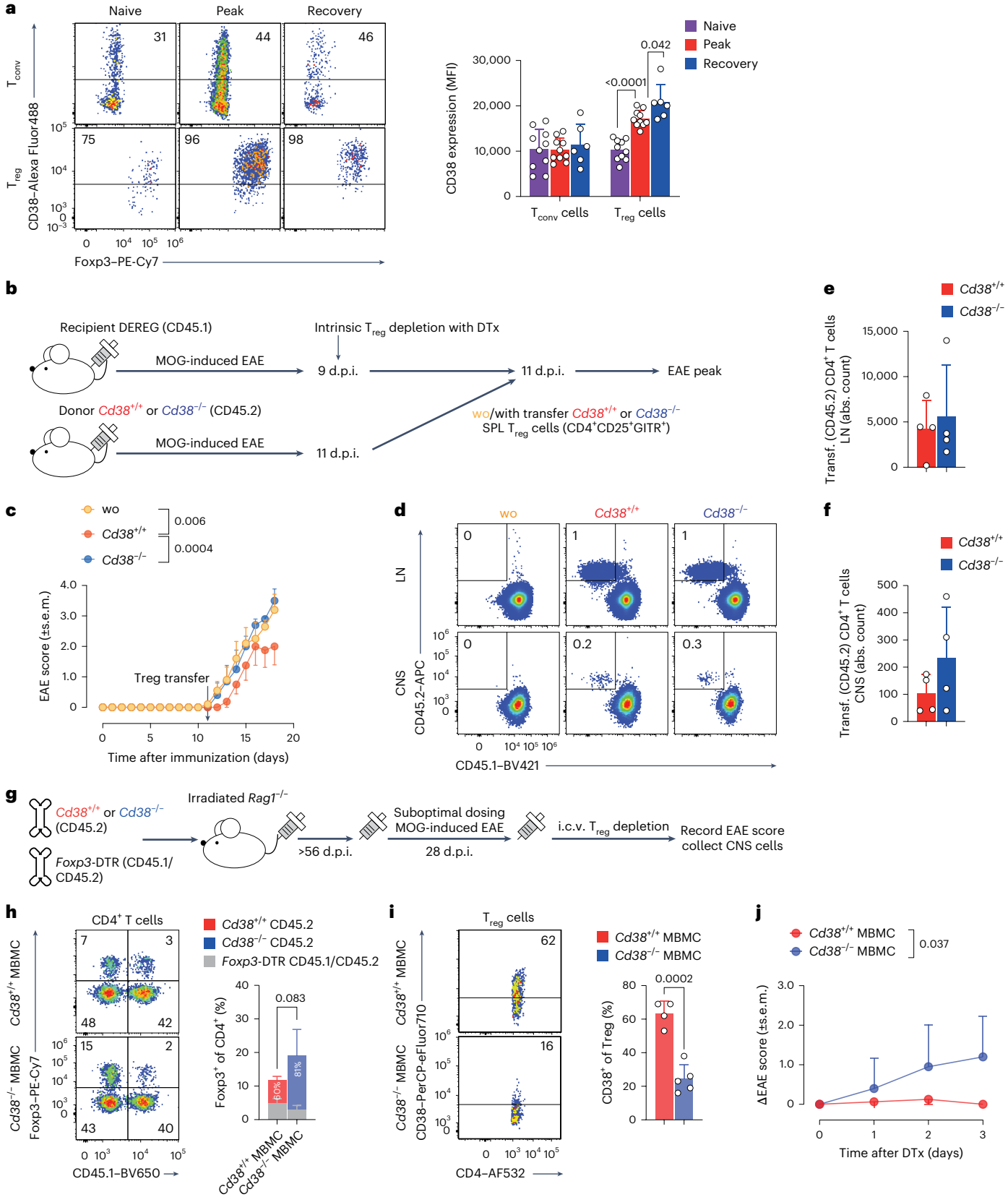

https://doi.org/10.1038/s41590-025-02416-z

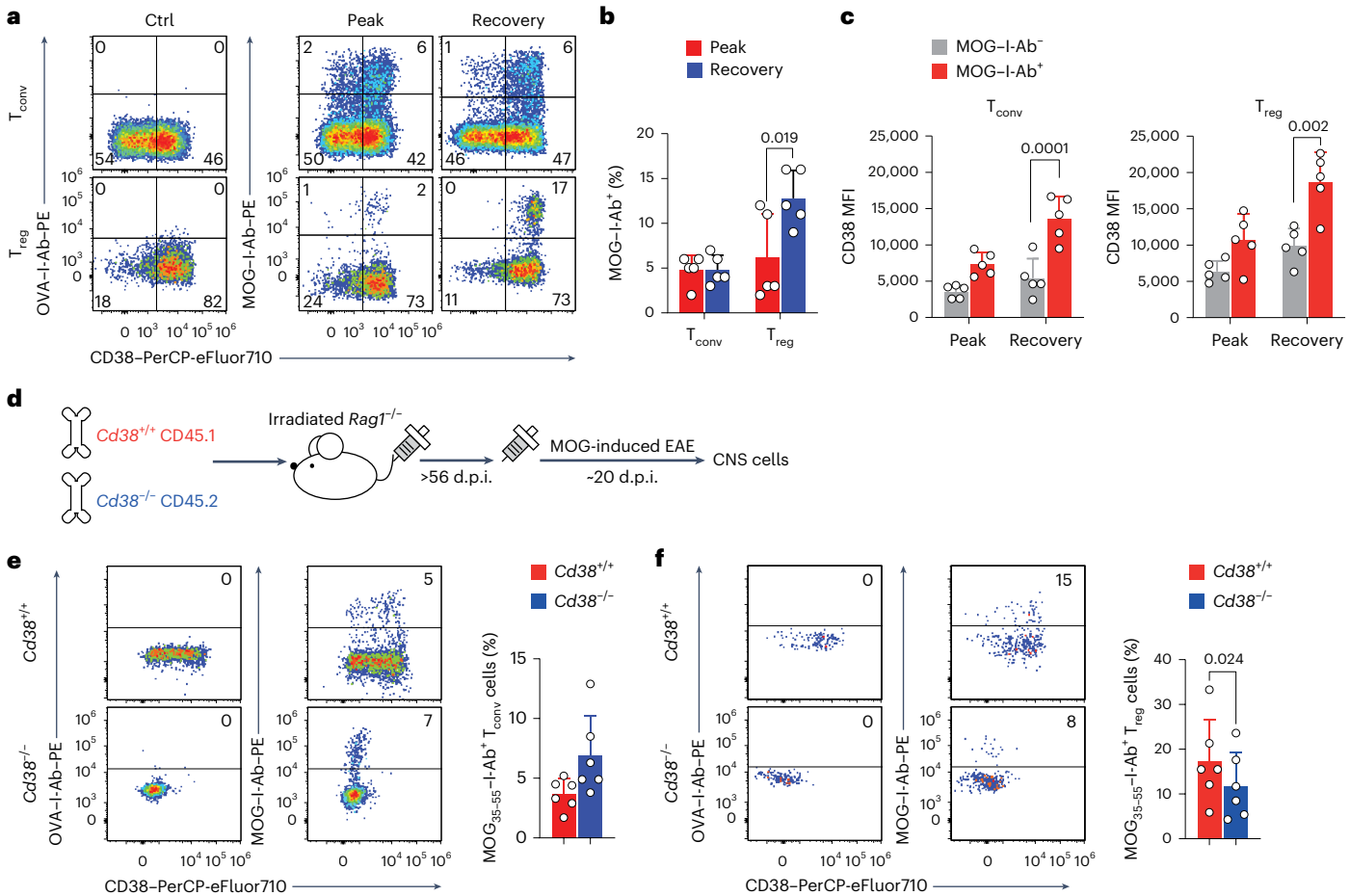

Fig. 7 | CD38 is essential for persistence of antigen-specific T_{reg} cells in the inflamed CNS. EAE was induced in wild-type C57BL/6 mice. **a**,**b**, Percentages of MOG–I-Ab tetramer-binding T_{conv} and T_{reg} cells in the CNS at different stages of EAE. **c**, CD38 expression in MOG–I-Ab$^-$ versus MOG–I-Ab$^+$ T_{conv} and T_{reg} cells across EAE stages. Each symbol in **b** and **c** represents an individual mouse. Data are shown as mean + s.d. *P* values were calculated using a two-way ANOVA with a Tukey's HSD test ($n = 5$ biological replicates). **d**, Mixed BM from *Cd38*$^{+/+}$ (CD45.1) and *Cd38*$^{-/-}$ (CD45.2) mice was transferred into sublethally irradiated *Rag1*$^{-/-}$ recipients. EAE was induced in BM-reconstituted mice, and CNS cells were collected 20 days after MOG_{35-55} immunization. Percentages of MOG–I-Ab-binding *Cd38*$^{+/+}$ CD45.1$^+$ and *Cd38*$^{-/-}$ CD45.2$^+$ T_{conv} (TCRβ$^+$CD4$^+$Foxp3$^-$; **e**) and T_{reg} cells (TCRβ$^+$CD4$^+$Foxp3$^+$; **f**). Each symbol in **e** and **f** represents an individual mouse. Data are shown as mean + s.d. The *P* value was calculated using a paired two-tailed Student's *t*-test ($n = 6$ biological replicates).

the defective immunosuppressive function of T_{reg} cells in individuals with multiple sclerosis[44]. Finally, T_{reg} cells require CD38 for adenosine synthesis via the CD38/CD203a/CD73 ectoenzymatic pathway[45]. Yet, we observed a physical loss of antigen-specific T_{reg} cells in the CNS when they lacked CD38 expression. Therefore, we suggest that CD38 is primarily necessary for the very maintenance of CNS T_{reg} cells in the chronically inflamed CNS because it enables them to exploit limited sources of IL-2. Prior studies are consistent with the idea that the availability of IL-2 defines the physical and functional niche of T_{reg} cells in nonlymphoid tissues[16].

The chronically inflamed CNS is characterized by a high load of extracellular NAD[+][21]. Therefore, we propose that CD38 expression by T_{reg} cells is a key feature that determines their resilience to the 'environmental' stress of this niche. In addition, CNS T_{reg} cells share much of what has been described as the tissue-resident T_{reg} cell signature[2,46]. It is unresolved whether a universal tissue T_{reg} cell signature can be defined or whether each tissue has its own unique T_{reg} cell population, both in terms of TCR repertoire and functional phenotype. Although other investigators have found a comparable T_{reg} cell TCR repertoire diversity in various tissue sites[6], these data need to be interpreted with caution as it is virtually impossible to reach the saturation limit in single-cell sequencing of a fully polyclonal repertoire with currently available technologies. Our data would argue in favor of the requirement for a cognate engagement of postinflammatory CNS-resident T_{reg} cells because the ablation of CD38 induces a more profound loss of MOG-specific T_{reg} cells than of T_{reg} cells that do not bind MOG_{35-55}–I-Ab tetramers. Therefore, the availability of tissue-specific private antigens may require antigen-specific T_{reg} cells, whose resilience to the local environment then depends on a universal tissue-type transcriptional program, including CD38.

Finally, local depletion of postinflammatory CNS T_{reg} cells was sufficient to provoke an EAE relapse, whereas systemic T_{reg} cell depletion was not. Postinflammatory T_{reg} cells are, thus, not only adapted to their tissue niche, where they may fulfill nonimmune functions[1,15,17,47], but also still absolutely essential to prevent the recurrence of inflammation in a metastable environment. In fact, CNS inflammation is rekindled from niches of persistent immune cells in the inflammation-experienced CNS when T_{reg} cells are ablated. These findings establish a paradigm that could explain the increasing disconnect of immunopathology from the systemic immune compartment in chronic CNS autoimmunity. Defining their local interaction partners and growth, as well as maintenance, factors will open new avenues for manipulating CNS T_{reg} cells as auditors of compartmentalized inflammatory processes that may drive immunopathology in progressive CNS autoimmunity.

https://doi.org/10.1038/s41590-025-02416-z

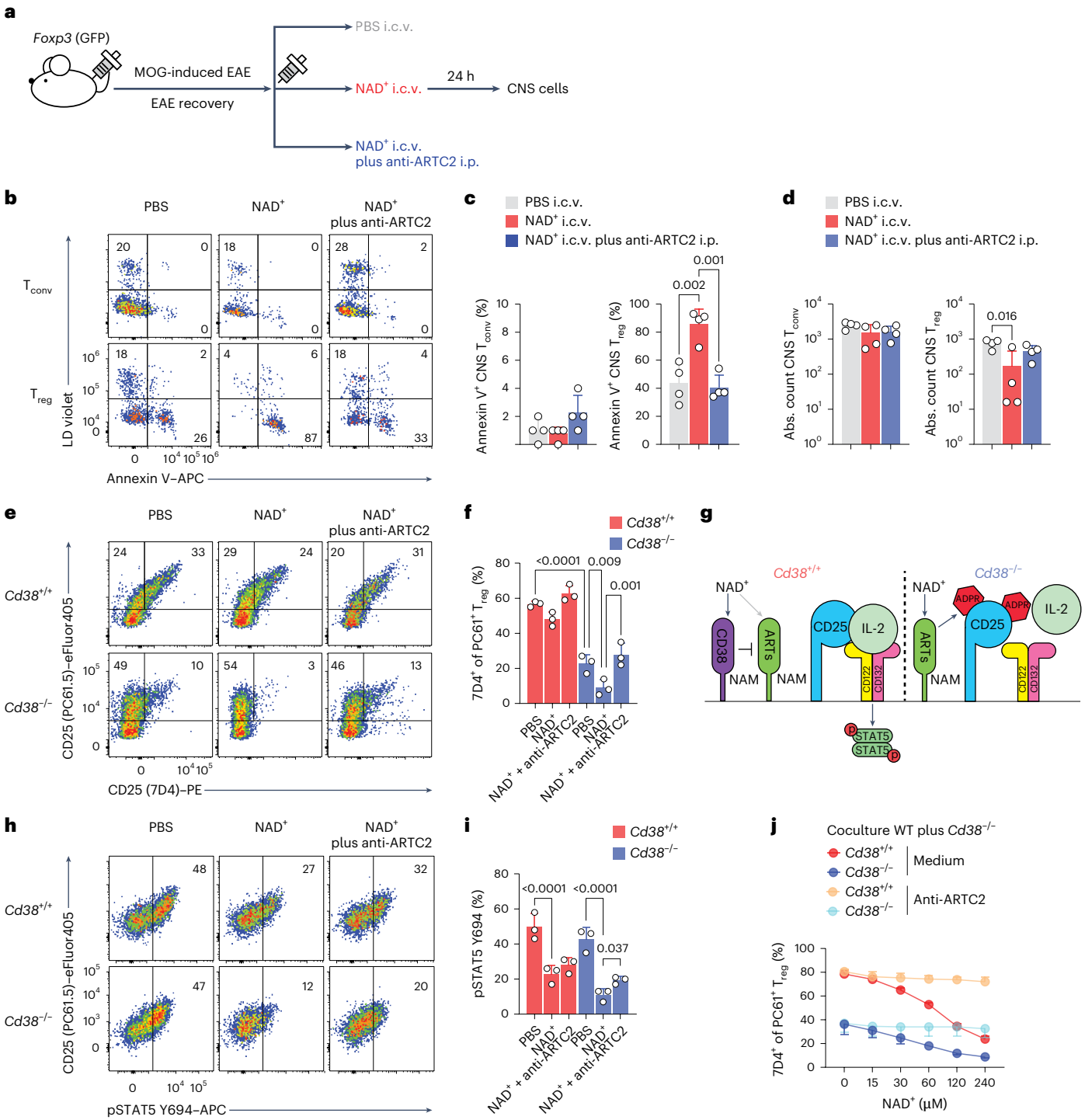

Fig. 8 | Stress-tolerant T_{reg} cells are dependent on CD38 for efficient IL-2 sensing. a,**b**, EAE was induced in *Foxp3* (GFP) mice. NAD^+ or PBS was administered i.c.v. (100 µg) with or without anti-ARTC2.2 i.p. injection (50 µg) during the recovery phase of EAE (**a**). Mice were killed 1 day after treatment, and Annexin V and LD Violet staining was performed on isolated CNS T_{conv} and T cells (**b**). **c**,**d**, Percentage of Annexin V^+ (**c**) and total counts of viable (Annexin V^-LD $Violet^-$) T_{conv} and T_{reg} cells (**d**). Each symbol in **c** and **d** represents an individual mouse. Data are shown as mean + s.d. *P* values were calculated using a one-way ANOVA followed by a Tukey's HSD test ($n = 4$ biological replicates). **e**, Splenocytes from *Cd38*$^{+/+}$ and *Cd38*$^{-/-}$ mice were preincubated with or without NAD^+ (30 µM) and anti-ARTC2.2 (1 µg ml^{-1}). $CD4^+Foxp3^+$ T_{reg} cells were analyzed for CD25 ADP-ribosylation using clones 7D4 and PC61.5 of anti-CD25 by flow cytometry. **f**, Percentage of $7D4^+$ within $PC61.5^+$ T_{reg} cells. Each symbol represents an individual mouse. Data are shown as mean + s.d. *P* values were calculated using a two-way ANOVA with a Tukey's HSD test ($n = 3$ biological replicates). **g**, Model for CD38 inhibiting the ADP-ribosylation (ADPR) of CD25: CD38 on T_{reg} cells metabolizes extracellular NAD^+, competitively inhibiting ADP-ribosyltransferase (ART) activity, thereby preserving the high-affinity IL-2R conformation and sustaining STAT5 phosphorylation; NAM, nicotinamide. **h**, As in **e**, following preincubation, cells were stimulated with mouse IL-2 (1.25 ng ml^{-1}) and analyzed for STAT5 Y694 phosphorylation (pSTAT5 Y694) in T_{reg} cells by flow cytometry. **i**, Percentage of pSTAT5 $Y694^+CD4^+Foxp3^+$ T_{reg} cells. Each symbol represents an individual mouse. Data are shown as mean + s.d. *P* values were calculated by a two-way ANOVA with a Tukey's HSD test ($n = 3$ biological replicates). **j**, *Cd38*$^{+/+}$ and *Cd38*$^{-/-}$ splenocytes were labeled with different anti-CD4 fluorochromes, mixed 1:1 (2.5×10^6 each) in the same well and incubated with a twofold serial titration of NAD^+ with or without anti-ARTC2.2 (1 µg ml^{-1}). The percentages of $7D4^+$ cells within the $PC61.5^+$ T_{reg} cell population are shown as mean + s.d. for the wild-type and CD38-deficient compartments ($n = 4$ biological replicates); WT, wild-type.

Online content

Any methods, additional references, Nature Portfolio reporting summaries, source data, extended data, supplementary information, acknowledgements, peer review information; details of author contributions and competing interests; and statements of data and code availability are available at https://doi.org/10.1038/s41590-025-02416-z.

References

1. Feuerer, M. et al. Lean, but not obese, fat is enriched for a unique population of regulatory T cells that affect metabolic parameters. *Nat. Med.* **15**, 930–939 (2009).
2. Panduro, M., Benoist, C. & Mathis, D. Tissue T_{reg}s. *Annu. Rev. Immunol.* **34**, 609–633 (2016).
3. Russler-Germain, E. V., Rengarajan, S. & Hsieh, C. S. Antigen-specific regulatory T-cell responses to intestinal microbiota. *Mucosal Immunol.* **10**, 1375–1386 (2017).
4. Li, C. et al. TCR transgenic mice reveal stepwise, multi-site acquisition of the distinctive fat-T_{reg} phenotype. *Cell* **174**, 285–299 (2018).
5. Korn, T. & Muschaweckh, A. Stability and maintenance of Foxp3$^+$ T_{reg} cells in non-lymphoid microenvironments. *Front. Immunol.* **10**, 2634 (2019).
6. Burton, O. T. et al. The tissue-resident regulatory T cell pool is shaped by transient multi-tissue migration and a conserved residency program. *Immunity* **57**, 1586–1602 (2024).
7. Delacher, M. et al. Single-cell chromatin accessibility landscape identifies tissue repair program in human regulatory T cells. *Immunity* **54**, 702–720 (2021).
8. DiSpirito, J.R. et al. Molecular diversification of regulatory T cells in nonlymphoid tissues. *Sci. Immunol.* **3**, eaat5861 (2018).
9. Fan, X. et al. CD49b defines functionally mature T_{reg} cells that survey skin and vascular tissues. *J. Exp. Med.* **215**, 2796–2814 (2018).
10. Abbas, A. K., Trotta, E., Dimitre, R. S., Marson, A. & Bluestone, J. A. Revisiting IL-2: biology and therapeutic prospects. **3**, eaat1482 (2018)
11. Korn, T. et al. Myelin-specific regulatory T cells accumulate in the CNS but fail to control autoimmune inflammation. *Nat. Med.* **13**, 423–431 (2007).
12. Cretney, E. et al. The transcription factors Blimp-1 and IRF4 jointly control the differentiation and function of effector regulatory T cells. *Nat. Immunol.* **12**, 304–311 (2011).
13. Garg, G. et al. Blimp1 prevents methylation of Foxp3 and loss of regulatory T cell identity at sites of inflammation. *Cell Rep.* **26**, 1854–1868 (2019).
14. Delacher, M. et al. Precursors for nonlymphoid-tissue T_{reg} cells reside in secondary lymphoid organs and are programmed by the transcription factor BATF. *Immunity* **52**, 295–312 (2020).
15. Ito, M. et al. Brain regulatory T cells suppress astrogliosis and potentiate neurological recovery. *Nature* **565**, 246–250 (2019).
16. Yshii, L. et al. Astrocyte-targeted gene delivery of interleukin 2 specifically increases brain-resident regulatory T cell numbers and protects against pathological neuroinflammation. *Nat. Immunol.* **23**, 878–891 (2022).
17. Dombrowski, Y. et al. Regulatory T cells promote myelin regeneration in the central nervous system. *Nat. Neurosci.* **20**, 674–680 (2017).
18. Shi, L. et al. T_{reg} cell-derived osteopontin promotes microglia-mediated white matter repair after ischemic stroke. *Immunity* **54**, 1527–1542 (2021).
19. Marin-Rodero, M. et al. The meninges host a distinct compartment of regulatory T cells that preserves brain homeostasis. *Sci. Immunol.* **10**, eadu2910 (2025).
20. Midavaine, E. et al. Meningeal regulatory T cells inhibit nociception in female mice. *Science* **388**, 96–104 (2025).
21. Chiarugi, A. Inhibitors of poly(ADP-ribose) polymerase-1 suppress transcriptional activation in lymphocytes and ameliorate autoimmune encephalomyelitis in rats. *Br. J. Pharmacol.* **137**, 761–770 (2002).
22. Aswad, F., Kawamura, H. & Dennert, G. High sensitivity of CD4$^+$CD25$^+$ regulatory T cells to extracellular metabolites nicotinamide adenine dinucleotide and ATP: a role for $P2X_7$ receptors. *J. Immunol.* **175**, 3075–3083 (2005).
23. Seman, M. et al. NAD-induced T cell death. *Immunity* **19**, 571–582 (2003).
24. Bettelli, E. et al. Reciprocal developmental pathways for the generation of pathogenic effector T_H17 and regulatory T cells. *Nature* **441**, 235–238 (2006).
25. Kim, E. H. et al. Bach2 regulates homeostasis of Foxp3$^+$ regulatory T cells and protects against fatal lung disease in mice. *J. Immunol.* **192**, 985–995 (2014).
26. Osman, A. et al. TCF-1 controls T_{reg} cell functions that regulate inflammation, CD8$^+$ T cell cytotoxicity and severity of colon cancer. *Nat. Immunol.* **22**, 1152–1162 (2021).
27. Lahl, K. et al. Selective depletion of Foxp3$^+$ regulatory T cells induces a scurfy-like disease. *J. Exp. Med.* **204**, 57–63 (2007).
28. Wakim, L. M., Woodward-Davis, A. & Bevan, M. J. Memory T cells persisting within the brain after local infection show functional adaptations to their tissue of residence. *Proc. Natl. Acad. Sci. USA* **107**, 17872–17879 (2010).
29. Zeidler, J. D. et al. Endogenous metabolism in endothelial and immune cells generates most of the tissue vitamin B3 (nicotinamide). *iScience* **25**, 105431 (2022).
30. Leutert, M. et al. Identification of the mouse T cell ADP-ribosylome uncovers ARTC2.2 mediated regulation of CD73 by ADP-ribosylation. *Front. Immunol.* **12**, 703719 (2021).
31. Stephens, L. A., Malpass, K. H. & Anderton, S. M. Curing CNS autoimmune disease with myelin-reactive Foxp3$^+$ T_{reg}. *Eur. J. Immunol.* **39**, 1108–1117 (2009).
32. Sabatino, J. J. Jr., Huang, J., Zhu, C. & Evavold, B. D. High prevalence of low affinity peptide–MHC II tetramer-negative effectors during polyclonal CD4$^+$ T cell responses. *J. Exp. Med.* **208**, 81–90 (2011).
33. Georgiev, H. et al. Blocking the ART2.2/$P2X_7$-system is essential to avoid a detrimental bias in functional CD4 T cell studies. *Eur. J. Immunol.* **48**, 1078–1081 (2018).
34. Teege, S. et al. Tuning IL-2 signaling by ADP-ribosylation of CD25. *Sci. Rep.* **5**, 8959 (2015).
35. Shubinsky, G. & Schlesinger, M. The CD38 lymphocyte differentiation marker: new insight into its ectoenzymatic activity and its role as a signal transducer. *Immunity* **7**, 315–324 (1997).
36. Chini, C. C. S., Zeidler, J. D., Kashyap, S., Warner, G. & Chini, E. N. Evolving concepts in NAD$^+$ metabolism. *Cell Metab.* **33**, 1076–1087 (2021).
37. Deaglio, S. et al. Human CD38 (ADP-ribosyl cyclase) is a counter-receptor of CD31, an Ig superfamily member. *J. Immunol.* **160**, 395–402 (1998).
38. Krebs, C. et al. CD38 controls ADP-ribosyltransferase-2-catalyzed ADP-ribosylation of T cell surface proteins. *J. Immunol.* **174**, 3298–3305 (2005).
39. Hubert, S. et al. Extracellular NAD$^+$ shapes the Foxp3$^+$ regulatory T cell compartment through the ART2–$P2X_7$ pathway. *J. Exp. Med.* **207**, 2561–2568 (2010).
40. Andrejew, R. et al. The $P2X_7$ receptor: central hub of brain diseases. *Front. Mol. Neurosci.* **13**, 124 (2020).
41. Covarrubias, A. J., Perrone, R., Grozio, A. & Verdin, E. NAD$^+$ metabolism and its roles in cellular processes during ageing. *Nat. Rev. Mol. Cell Biol.* **22**, 119–141 (2021).

42. Beier, U. H., Akimova, T., Liu, Y., Wang, L. & Hancock, W. W. Histone/protein deacetylases control Foxp3 expression and the heat shock response of T-regulatory cells. *Curr. Opin. Immunol.* **23**, 670–678 (2011).
43. Huang, X. & Rudensky, A. Y. Regulatory T cells in the context: deciphering the dynamic interplay with the tissue environment. *Curr. Opin. Immunol.* **89**, 102453 (2024).
44. Schwarz, A. et al. Fine-tuning of regulatory T cell function: the role of calcium signals and naive regulatory T cells for regulatory T cell deficiency in multiple sclerosis. *J. Immunol.* **190**, 4965–4970 (2013).
45. Horenstein, A. L. et al. A CD38/CD203a/CD73 ectoenzymatic pathway independent of CD39 drives a novel adenosinergic loop in human T lymphocytes. *Oncoimmunology* **2**, e26246 (2013).
46. Burzyn, D., Benoist, C. & Mathis, D. Regulatory T cells in nonlymphoid tissues. *Nat. Immunol.* **14**, 1007–1013 (2013).
47. Vasanthakumar, A. et al. The transcriptional regulators IRF4, BATF and IL-33 orchestrate development and maintenance of adipose tissue-resident regulatory T cells. *Nat. Immunol.* **16**, 276–285 (2015).

[1]Institute for Experimental Neuroimmunology, Technical University of Munich School of Medicine, Munich, Germany. [2]Department of Biotechnology and Bioinformatics, School of Life Sciences, University of Hyderabad, Hyderabad, India. [3]Institute of Pathology, Technical University of Munich, Munich, Germany. [4]Department of Pathology and Immunology, Division of Clinical Pathology, Geneva Faculty of Medicine, Centre Médical Universitaire, Geneva, Switzerland. [5]Institute for Computational Biology, Helmholtz Munich, Campus Neuherberg, Neuherberg, Germany. [6]Institute of Molecular Oncology and Functional Genomics, TranslaTUM Cancer Center, Technical University of Munich School of Medicine, Munich, Germany. [7]Department of Neurology, Technical University of Munich School of Medicine, Munich, Germany. [8]Division of Molecular Biology, Biomedical Center, Faculty of Medicine, LMU Munich, Martinsried, Germany. [9]Munich Cluster for Systems Neurology, Munich, Germany. [10]These authors jointly supervised this work: Andreas Muschaweckh, Thomas Korn. ✉e-mail: thomas.korn@tum.de

Methods

Mice

Foxp3$^{eGFP\text{-}Cre\text{-}ERT2}$ (*Foxp3*$^{Cre\text{-}ERT2}$, IMSR_JAX:016961)[48], *Foxp3*^{DTR} (*Foxp3*-DTR, IMSR_JAX:016958)[49], CD45.1 congenic (IMSR_JAX:002014)[50] and B6.129S7-*Rag1*$^{tm1Mom/J}$ (*Rag1*$^{-/-}$, IMSR_JAX:002216)[51] mice were obtained from The Jackson Laboratory. C57BL/6J (wild-type, IMSR_JAX:000664) mice were from Charles River Laboratories. *Foxp3* (GFP) reporter mice[24] were provided by V. Kuchroo (Harvard Medical School and Brigham and Women's Hospital). *Cd38*^{tm1Lnd} (*Cd38*$^{-/-}$, IMSR_JAX:003727) mice[52] were provided by H.-W. Mittrücker (Medical Center Hamburg Eppendorf). *Foxp3*$^{Cre\text{-}ERT2}$ mice and *Rosa*-CAG-LSL-tdTomato-WPRE::ΔNeo mice (*Rosa26*$^{LSL\text{-}tdTomato}$, IMSR_JAX:007914)[53] were mated to generate *Foxp3*$^{Cre\text{-}ERT2}$ × *Rosa26*$^{LSL\text{-}tdTomato}$ mice. *Pham*^{T} reporter mice (*Cd4*^{Cre} × *Rosa26*$^{LSL\text{-}mitoDendra2}$, that is, IMSR_JAX:022071 mated with IMSR_JAX:018385) were generated in-house[54]. DEREG mice (MMRRC_032049-JAX)[27] were provided by T. Sparwasser (University Medical Center Mainz). We used 8- to 20-week-old disease score-matched male and female C57BL/6 mice in all experiments (see Hiltensperger et al.[54]), except for VAT, where we only used 20-week-old male mice[55]. Mice were housed in a specific pathogen-free facility with normal rodent chow at the Technical University of Munich. Protocols were approved by the Bavarian state authorities and conducted according to the relevant guidelines (ROB-55.2-2532.Vet_02-17-69, ROB-55.2-2532.Vet_02-17-234, ROB-55.2-2532.Vet_03-18-53, ROB-55.2-2532.Vet_02-20-1, ROB-55.2-2532.Vet_02-20-23, ROB-55.2-2532.Vet_02-20-187, ROB-55.2-2532.Vet_02-23-71, ROB-55.2-2532.Vet_02-23-118 and ROB-55.2-2532.Vet_02-25-68).

EAE model

Mice were immunized with $MOG_{35–55}$ (200 µg, Auspep) emulsified in complete Freund's adjuvant (500 mg *Mycobacterium tuberculosis* H37Ra, BD Difco). Mice received 200 ng or a suboptimal dose of 50 ng pertussis toxin (Sigma-Aldrich) i.v. on days 0 and 2 after immunization. Clinical scores were recorded as 0 (no disease), 1 (tail tone loss), 2 (hind limb paresis), 3 (hind limb paralysis), 4 (tetraplegia) and 5 (moribund). Peak disease occurred on days 12–15, with recovery starting around days 30–35.

BM chimeras

Six- to 8-week-old *Rag1*$^{-/-}$ mice were sublethally irradiated (7 Gy; two doses of 3.5 Gy, 3 h apart) and i.v. injected with 1×10^7 CD90.2-depleted donor BM cells. Mice received enrofloxacin (0.1 mg ml^{-1}) in their drinking water for 2 weeks after BM transplantation. Hematopoietic reconstitution was assessed using peripheral blood at 6 weeks, and the chimeras were immunized for EAE induction 8 weeks after BM grafting.

Tissue and cell isolation

Mice were killed and perfused with 20–30 ml of cold PBS via the left heart ventricle. Spleen tissue and lymph nodes were homogenized and filtered (70-µm strainers, Falcon), and red blood cells were lysed with 2 ml of FACS Lysing Solution (BD Biosciences) for 5 min. Cells were washed and resuspended in FACS buffer (2% fetal calf serum (FCS) in PBS). For CNS cell isolation, brains were dissected, and spinal cords were flushed out with PBS. CNS tissues were digested in 4 ml of digestion buffer (2.5 mg ml^{-1} collagenase D (Roche Diagnostics), 1 mg ml^{-1} DNase I (Roche Diagnostics) and 1 µg ml^{-1} S+16a anti-ARTC2.2 nanobody (BioLegend) in 10% FCS DMEM) at 37 °C for 45 min with shaking at 120 rpm, filtered and separated via Percoll gradient (70–37%, GE Healthcare). Cells were collected, washed and resuspended in cold FACS buffer. VAT from male mice was collected, digested in 3 ml of digestion buffer at 37 °C for 45 min, washed with 30 ml of FACS buffer and treated with 1 ml of FACS lysing solution for 5 min. Cells were washed, pelleted and resuspended in cold FACS buffer. BM was isolated from the femur and tibia. The bones were cut out from each end and flushed out with cold 10% FCS DMEM with a 21-gauge needle. The cells were collected, and red blood cells were lysed with 1 ml of FACS lysing solution for 5 min. The cells were then washed and resuspended in cold FACS buffer.

Cell sorting

Splenocytes and lymph nodes were pooled to isolate T_{reg} cells. Briefly, CD4$^+$ T cells were enriched from single-cell suspensions using a negative selection kit (Miltenyi Biotec). Cells were stained with antibodies for 15 min at 4 °C in the dark, washed and resuspended in FACS buffer. Sorting was conducted using a FACSAria III Cell Sorter (BD Biosciences), achieving >95% purity.

Flow cytometry

Cell suspensions were stained with Live/Dead Aqua, Live/Dead violet or Near-IR dyes (Thermo Fisher) for 15 min at 4 °C in PBS and washed with FACS buffer. Cells were incubated with an antibody cocktail targeting surface antigen and CD16/CD32 Fc block in FACS buffer for 15 min at 4 °C in the dark, washed twice and resuspended in FACS buffer. For Annexin V staining, cells were stained with an antibody cocktail in Annexin V binding buffer (BioLegend). For intracellular staining, cells were stained with antibodies to surface antigens, fixed with 4% paraformaldehyde (PFA) for 15 min at room temperature (protected from light) and washed with FACS buffer. Fixation and permeabilization were performed using a eBioscience Intracellular Fixation and Permeabilization Buffer Set (Invitrogen). Cells were incubated overnight at 4 °C with an intracellular antibody cocktail and Fc block in permeabilization buffer, washed and resuspended in FACS buffer.

For pSTAT5 Y694 staining, fixation and permeabilization were performed using a Transcription Factor Phospho Buffer Set (TFP, BD Pharmingen), following the manufacturer's protocol. In short, after fixation and permeabilization, cells were incubated with anti-pSTAT5 Y694, anti-Foxp3 and anti-surface antigen with Fc block in TFP Perm/Wash Buffer for 50 min at 4 °C. Cells were washed twice with TFP Perm/Wash buffer and resuspended in FACS buffer for flow cytometry analysis. A list of the applied antibodies and resources is provided in Supplementary Table 4. Antibody dilutions are detailed in the Reporting Summary. Data were collected using CytoFLEX (Beckman Coulter), FACSAria III (BD Biosciences) or Aurora (Cytek Biosciences) and analyzed using FlowJo software (version 10.8.1, BD Biosciences).

T_{reg} cell cluster visualizations were based on the data acquired on the Aurora system. T_{reg} cells were identified as Aqua$^-$Foxp3$^+$CD4$^+$ through primary gating in each sample in FlowJo. To standardize cell numbers across tissues, downsampling was conducted by pooling and selecting 300 T_{reg} cells, which were then subjected to secondary FlowSOM (v3.0.18) clustering. Further subclustering of T_{reg} cells was achieved using ClusterExplorer (v1.6.5). The clusters were visualized with uniform manifold approximation and projection through R and the FlowJo plugin packages.

I-Ab tetramer staining

CNS and spleen cells were treated with neuraminidase (0.35 U ml^{-1}, Sigma-Aldrich) and dasatinib (100 nM, Selleckchem) in serum-free DMEM at 37 °C with 5% CO_2 for 25 min. Cells were then washed twice with FACS buffer, blocked with anti-mouse CD16/CD32 Fc block on ice for 15 min and stained with T-Select I-A^b $MOG_{35–55}$ Tetramer-PE (Medical and Biological Laboratories, TS-M704-1) or the control T-Select I-A^b $OVA_{323–339}$ Tetramer-PE (TS-M710-1) at room temperature for 2 h, with gentle resuspension every 30 min. After tetramer staining, cells were centrifuged (430*g*, 4 °C, 5 min), washed twice with FACS buffer and incubated with anti-phycoerythrin MicroBeads (Miltenyi Biotec) on a 4 °C shaker for 30 min to stabilize tetramer binding. The cells were washed with FACS buffer and subjected to surface and intracellular staining for flow cytometry analysis. The tetramer$^+$ population was identified by gating on NIR$^-$, Lin (CD19, CD8a, F4/80, Ly6G)$^-$ and $MOG_{35–55}$ tetramer–PE$^+$ cells, with the $OVA_{323–339}$ tetramer as a negative control.

Bulk RNA-seq

Approximately 2,000 or 250 T_{reg} or T_{conv} cells (viability > 90%) were sorted directly into TCL buffer (Qiagen) plus 1% 2-mercaptoethanol

(Merk) and stored at −80 °C. RNA was extracted and purified using an RNeasy Plus Micro kit (Qiagen). RNA quality was assessed using an Agilent 2100 Bioanalyzer (Agilent Technologies). Library preparation followed a previously described protocol[56]. Barcode-specific cDNA was synthesized via reverse transcription with Maxima RT polymerase (Thermo Fisher) using an oligo(dT) primer containing barcodes, unique molecular identifiers (UMIs) and adaptor sequences. The 5′ end of the cDNA was then extended using primers complementary to the template switch oligonucleotide site, followed by amplification of full-length cDNA. The cDNA was fragmented using a Nextera XT kit (Illumina), and the 3′-end fragments were amplified with primers incorporating Illumina P5 and P7 overhangs. The P5 and P7 sites were modified to optimize cluster recognition during sequencing, allowing for sequencing of the cDNA in read 1 and the barcodes/UMIs in read 2.

Sequencing was performed on an Illumina NextSeq 500 platform with 75 cycles for read 1 and 16 for read 2. The sequencing data were processed using the Drop-seq pipeline[57] to generate UMI tables organized by sample and gene. The GRCm38 reference genome was aligned with transcript and gene annotations derived from ENSEMBL release 75.

Differential gene expression analysis was conducted in R (v4.5.0) using the DESeq2 package (v1.48.1)[58]. Significant DEGs were defined as genes with a Benjamini–Hochberg-adjusted *P* value of <0.05 (in some cases 0.1 as indicated) and an absolute fold change in expression of >1.5. A $\log_2$(fold shrinkage) estimation was performed using the R package glmGamPoi (v1.20.0)[59]. GO term annotations were derived from the R package org.Mm.eg.db (v3.21.0). For visualization, count data were transformed using the variance stabilizing transformation ('vst') function in DESeq2. GSEA was performed on DESeq2 normalized counts using the Broad Institute GSEA Desktop Application (v4.3.2) in conjunction with the Molecular Signatures Database (v2024.1.Mm), with permutation type 'gene_set' and an FDR threshold of 0.25 applied. GO enrichment analysis of adjusted *P* value ranked DEGs was performed using the gprofiler2 R package[60].

In vivo cell proliferation assay

EAE was induced in C57BL/6 wild-type mice. At various time points during EAE progression, EdU (0.05 µg mg (body weight), Click-iT EdU, Sigma-Aldrich) was administered i.p. 18 h before euthanasia. Circulating cells were labeled with anti-CD45.2 BV650 (3 µg, BioLegend) via i.v. injection 3–5 min before euthanasia. EdU staining was performed according to the manufacturer's protocol. Cells from the CNS and spleen were stained with surface antigens and fixed with 4% PFA (Thermo Fisher) at room temperature for 15 min in the dark. After two washes with FACS buffer, cells were incubated in a saponin-based fixation-permeabilization buffer at room temperature for 20 min, followed by centrifugation. A fresh EdU detection cocktail was prepared, and cells were incubated at room temperature for 30 min. After two washes with the saponin-based fixation-permeabilization buffer, cells were stained with anti-Foxp3 in the same buffer overnight at 4 °C. Cells were washed twice again, resuspended in FACS buffer and analyzed by flow cytometry.

In vivo T cell trafficking assay

Mice were anesthetized with a cocktail of medetomidine, midazolam and fentanyl, and the fur was removed using depilatory cream (Veet). For photolabeling, the inguinal lymph node on the immunization side was irradiated for 20 min using a 405-nm diode laser (LuxX 405-60, Soliton) as previously described[54]. Two days after photoconversion, the mice were killed, and cells from the CNS and spleen were collected to assess the migration of photolabelled lymphocytes.

In vivo Foxp3 fate mapping

For tamoxifen preparation, tamoxifen (Sigma-Aldrich) was dissolved in 100% ethanol (Merck) at a concentration of 1 g ml^{-1}, vortexed at 37 °C for 15 min and mixed with Miglyol (Caelo) to achieve a final concentration of 10 mg ml^{-1}. The solution was incubated and vortexed at 37 °C for 30 min to ensure complete dissolution. We followed the protocol by Jahn et al.[61] for tamoxifen treatment. *Foxp3*$^{Cre\text{-}ERT2}$ × *Rosa26*$^{LSL\text{-}tdTomato}$ mice were given daily i.p. injections of 1 mg 100 $µl^{-1}$ tamoxifen for 5 days. Fourteen days after the last injection, the mice were killed, and their spleen and CNS cells were collected for either flow cytometry or RNA-seq analysis.

In vivo T_{reg} cell depletion

EAE was induced in *Foxp3*-DTR and control *Foxp3* (GFP) mice. During the EAE recovery phase (between 32 and 35 days after immunization, with a clinical score of less than 2), DTx (from *Corynebacterium diphtheriae*, Sigma-Aldrich) or PBS was administered either i.c.v. (15 ng) or i.p. (500 ng). The i.c.v. injection was performed according to the protocol described by Taylor et al.[62], modified to administer 3 µl of DTx at a rate of 1 µl min^{-1}. Buprenorphine (0.1 µg per mg (body weight)) was given before, after and 1 day after surgery for pain management. T_{reg} cell depletion efficiency was confirmed by flow cytometry, and clinical scores were monitored daily from day 0 to day 3 after DTx injection. For FTY720 treatment, FTY720 (1 µg per mg (body weight), Sigma-Aldrich) or vehicle control was administered i.p. starting 1 day before the DTx i.c.v. injection and continuing daily until 1 day after surgery. Clinical scores were recorded from day 0 to day 3.

In vivo T_{reg} cell suppression

EAE was induced in both donor (either *Cd38*$^{+/+}$ or *Cd38*$^{-/-}$, CD45.2) and recipient DEREG (CD45.1) mice. DTx (1 µg, 50 µg per kg (body weight)) was administered i.p. on days 9 and 10 after induction to deplete T_{reg} cells in recipients. On day 11, donors were pretreated i.p. with 50 µg of S+16a (anti-ARTC2.2 nanobody, BioLegend) 30 min before euthanasia to prevent cell apoptosis. Donor splenic T_{reg} cells (LIVE/DEAD Aqua$^-$ CD4$^+$CD25 (clone 7D4)$^+$GITR$^+$CD45.2$^+$) were sorted, and 10^5 T_{reg} cells were transferred i.v. into recipients.

In vivo NAD^+ i.c.v. injection

EAE was induced in *Foxp3* (GFP) mice. During the recovery phase, mice received an i.c.v. injection of either freshly prepared NAD^+ (Thermo Fisher; 100 µg in 3 µl of cold PBS) or vehicle control (3 µl of PBS). Buprenorphine (0.1 µg per mg (body weight)) was administered before and after surgery. Mice were killed 24 h after injection.

In vitro NAD^+ incubation and IL-2 stimulation

Splenocytes (5×10^6) from *Cd38*$^{+/+}$ or *Cd38*$^{-/-}$ mice were incubated with or without NAD^+ (concentrations are specified in the figure legends) and anti-ARTC2.2 (1 µg ml^{-1}) in serum-free DMEM at 4 °C for 15 min. Cells were washed with cold FACS buffer, stained with antibodies and analyzed by flow cytometry. For the pSTAT5 Y694 assay, following the initial incubation, cells were stimulated with mouse IL-2 (Miltenyi Biotec, 1.25 ng ml^{-1}) in DMEM containing 2% BSA at 37 °C for 10 min. Cells were immediately fixed and stained for anti-pSTAT5 Y694.

Histological analysis

Mice were killed and perfused with 20–30 ml of cold PBS via the left ventricle. Brains were dissected and fixed in 4% PFA at 4 °C for 48 h, washed with PBS and paraffin embedded. Representative 2-µm sections were cut with a rotary microtome, and immunohistochemistry was conducted using a Leica Bond Rxm autostainer with a Bond Polymer Refine Detection kit (DS9800, Leica Biosystems). Heat-induced epitope retrieval was performed by using citrate-based pH 6 Bond Epitope Retrieval Solution 1 (AR9961, Leica Biosystems). Antibody details are listed in Supplementary Table 4. Slides were then scanned with a Leica Aperio AT2 system and analyzed in QuPath (v0.6.0) using automated positive cell detection.

To generate multiplex immunostainings, 2-µm sections were deparaffinized and subjected to antigen retrieval (citrate buffer pH 6.0). To prevent myelin autofluorescence, slides were treated with

4.5% H_2O_2 and 20 mM NaOH in PBS under a light-emitting diode for 45 min twice at room temperature. Nonspecific binding was blocked with 2.5% goat serum in PBS, and samples were incubated overnight with rabbit anti-CD4 (Cell Signaling). Signals were detected with anti-rabbit horseradish peroxidase (Dako, K4003) with amplification (TSA vivid 520, Tocris, 7534). Following denaturation (Discovery Roche, CC2), slides were blocked with Fab fragment anti-mouse IgG (Jackson Immunoresearch) and 2.5% goat serum in PBS and incubated with rat anti-Foxp3 (eBioscience) overnight. Signals were detected with anti-rat horseradish peroxidase (Vectorlab) with amplification (TSA vivid 570, Tocris, 7535). Nuclei were stained with DAPI (Invitrogen), and slides were mounted in Fluoromount aqueous mounting medium (Sigma-Aldrich, F4680). Immunostained sections were scanned using an Akoya PhenoImager HT 2.0 (Akoya Biosciences).

For cryosections, brains were fixed in 4% PFA at 4 °C for 48 h and subjected to a 30% sucrose gradient for 48 h. Ten-micron cryosections (CM3050 S, Leica) were subjected to immunofluorescence stainings. The antibody details are listed in Supplementary Table 4. Images were acquired on an SP8 confocal microscope (Leica) and analyzed using LAS X software (v.3.5.6.21594, Leica).

Statistical analysis

Statistical analyses were performed using Prism 10 (GraphPad) or R (v4.4.0). No statistical methods were used to predetermine sample sizes, but our sample sizes were similar to those reported in previous publications[54]. Data distribution was assumed to be normal, but this was not always formally tested. In any case, individual data points are provided in the figures. Significance of the differences between two groups was evaluated using two-tailed Student's *t*-tests. Differences among three or more groups were analyzed using a one-way or two-way ANOVA with a Tukey's HSD post hoc test, and results are presented as mean values + s.d. Adjusted *P* values from DEGs were derived from DESeq2 using a two-tailed Wald's test with correction for multiple testing using the Benjamini and Hochberg method. Unless stated otherwise in the figure legend, animals were assigned to experimental groups in an age- and sex-matched manner. Scoring of EAE was performed in a manner blinded to the experimental conditions. Unless otherwise stated in the figure legends, all animals were included in the analysis. The significance of differences in clinical scores was determined using two-way ANOVA with a Tukey's post hoc test, and the results are presented as mean values + s.e.m. The significance of the survival rate was analyzed with a Mantel–Cox test. The individual sample sizes and statistical methods are provided in the figure legends. The individual *P* or adjusted *P* values are indicated in the figures.

Reporting summary

Further information on research design is available in the Nature Portfolio Reporting Summary linked to this article.

Data availability

Sequencing data have been deposited in the Gene Expression Omnibus database under accession code GSE311963. All other data are present in the article and Supplementary Information. Source data are provided with this paper.

References

48. Rubtsov, Y. P. et al. Stability of the regulatory T cell lineage in vivo. *Science* **329**, 1667–1671 (2010).
49. Kim, J. M., Rasmussen, J. P. & Rudensky, A. Y. Regulatory T cells prevent catastrophic autoimmunity throughout the lifespan of mice. *Nat. Immunol.* **8**, 191–197 (2007).
50. Shen, F. W. et al. Cloning of Ly-5 cDNA. *Proc. Natl Acad. Sci. USA* **82**, 7360–7363 (1985).
51. Mombaerts, P. et al. RAG-1-deficient mice have no mature B and T lymphocytes. *Cell* **68**, 869–877 (1992).
52. Cockayne, D. A. et al. Mice deficient for the ecto-nicotinamide adenine dinucleotide glycohydrolase CD38 exhibit altered humoral immune responses. *Blood* **92**, 1324–1333 (1998).
53. Madisen, L. et al. A robust and high-throughput Cre reporting and characterization system for the whole mouse brain. *Nat. Neurosci.* **13**, 133–140 (2010).
54. Hiltensperger, M. et al. Skin and gut imprinted helper T cell subsets exhibit distinct functional phenotypes in central nervous system autoimmunity. *Nat. Immunol.* **22**, 880–892 (2021).
55. Vasanthakumar, A. et al. Sex-specific adipose tissue imprinting of regulatory T cells. *Nature* **579**, 581–585 (2020).
56. Parekh, S., Ziegenhain, C., Vieth, B., Enard, W. & Hellmann, I. The impact of amplification on differential expression analyses by RNA-seq. *Sci. Rep.* **6**, 25533 (2016).
57. Macosko, E. Z. et al. Highly parallel genome-wide expression profiling of individual cells using nanoliter droplets. *Cell* **161**, 1202–1214 (2015).
58. Love, M. I., Huber, W. & Anders, S. Moderated estimation of fold change and dispersion for RNA-seq data with DESeq2. *Genome Biol.* **15**, 550 (2014).
59. Ahlmann-Eltze, C. & Huber, W. glmGamPoi: fitting γ-Poisson generalized linear models on single cell count data. *Bioinformatics* **36**, 5701–5702 (2021).
60. Kolberg, L., Raudvere, U., Kuzmin, I., Vilo, J. & Peterson, H. gprofiler2—an R package for gene list functional enrichment analysis and namespace conversion toolset g:Profiler. *F1000Res* **9**, ELIXIR-709 (2020).
61. Jahn, H. M. et al. Refined protocols of tamoxifen injection for inducible DNA recombination in mouse astroglia. *Sci. Rep.* **8**, 5913 (2018).
62. Taylor, Z. V., Khand, B., Porgador, A., Monsonego, A. & Eremenko, E. An optimized intracerebroventricular injection of $CD4^+$ T cells into mice. *STAR Protoc.* **2**, 100725 (2021).

Acknowledgements

We are grateful to H.-W. Mittrücker (Universitätsklinikum Hamburg Eppendorf) for generously providing CD38-deficient mice. We would like to thank K. Schumann (University of Konstanz) and M. Schmidt-Supprian (Technical University of Munich School of Medicine) for fruitful discussions. We appreciate B. Lunk, M. Schmidt and V. Husterer (all Technical University of Munich School of Medicine) for their assistance with mouse colony management. We thank the Technical University of Munich Comparative Experimental Pathology Unit for expert support with histological analyses. This study was supported by the Deutsche Forschungsgemeinschaft (TRR274 (ID 408885537) to T.K., TRR355 (ID 490846870) to T.K. and A.M., GRK2668 (ID 435874434) to T.K. and EXC 2145 (SyNergy, ID 390857198) to T.K.) and by the Hertie Network of Clinical Neuroscience (to T.K.).

Author contributions

Conceptualization: H.-H.C., A.M. and T.K. Methodology: H.-H.C., S.T., D.R.N., R.K., T.G., I.W., H.D.M., I.B.-P., R.Ö., A.M.A., S.H., L.C.R., C.S., G.L., L.S., K.S., D.M., R.R., G.S. and B.S. Investigation: H.-H.C., S.T., D.R.N., R.K., T.G., I.W., H.D.M., A.M.A., S.H., L.C.R. and L.S. Visualization: H.-H.C., A.M. and T.K. Funding acquisition: A.M. and T.K. Supervision: A.M. and T.K. Writing, original draft: H.-H.C., A.M. and T.K. Writing, review and editing: A.M. and T.K.

Funding

Open access funding provided by Technische Universität München.

Competing interests

The authors declare no competing interests.

Additional information

Extended data is available for this paper at https://doi.org/10.1038/s41590-025-02416-z.

Supplementary information The online version contains supplementary material available at https://doi.org/10.1038/s41590-025-02416-z.

Correspondence and requests for materials should be addressed to Thomas Korn.

Peer review information *Nature Immunology* thanks Adrian Liston, Scott Zamvil and the other, anonymous, reviewer(s) for their contribution to the peer review of this work. Peer reviewer reports are available. Primary Handling Editor: Nick Bernard, in collaboration with the *Nature Immunology* team.

https://doi.org/10.1038/s41590-025-02416-z

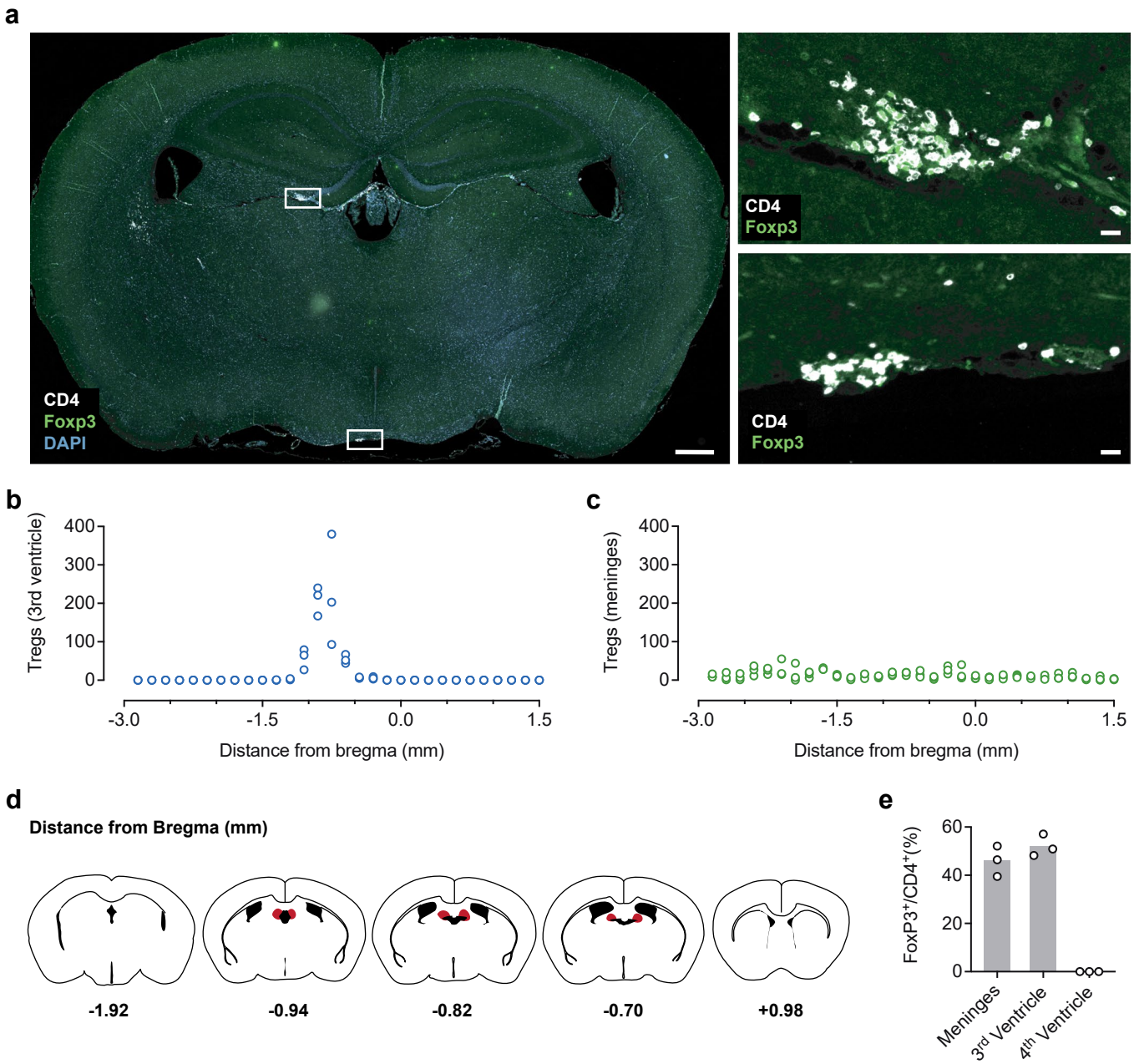

Extended Data Fig. 1 | Stress-tolerant Treg cells populate distinct niches in the chronically inflamed CNS. EAE was induced in *Foxp3* (GFP) mice, and on day 45 after MOG_{35-55} immunization, CNS tissue was collected, and serial sections of the brain were analyzed for the presence of $CD4^+Foxp3^+$ T cells (**a**). Representative coronal section, scale bar, overview 500 µm; scale bars, high power magnifications 50 µm. (**b**, **c**) Absolute number of Treg cells per coronal section in relation to the distance from the bregma, around the third ventricle (**b**) or the meningeal space (**c**). (**d**) Visualization of the Treg cell hotspot in the third ventricle area in coronal mouse brain atlas schemes (according to Paxinos and Franklin, The mouse brain in stereotaxic coordinates). (**e**) Quantification of $Foxp3^+$ Treg cells as a fraction of all $CD4^+$ T cells in the third ventricle area and the meningeal space. (**b**, **c**, **e**) Sample size: n = 3 biological replicates.

https://doi.org/10.1038/s41590-025-02416-z

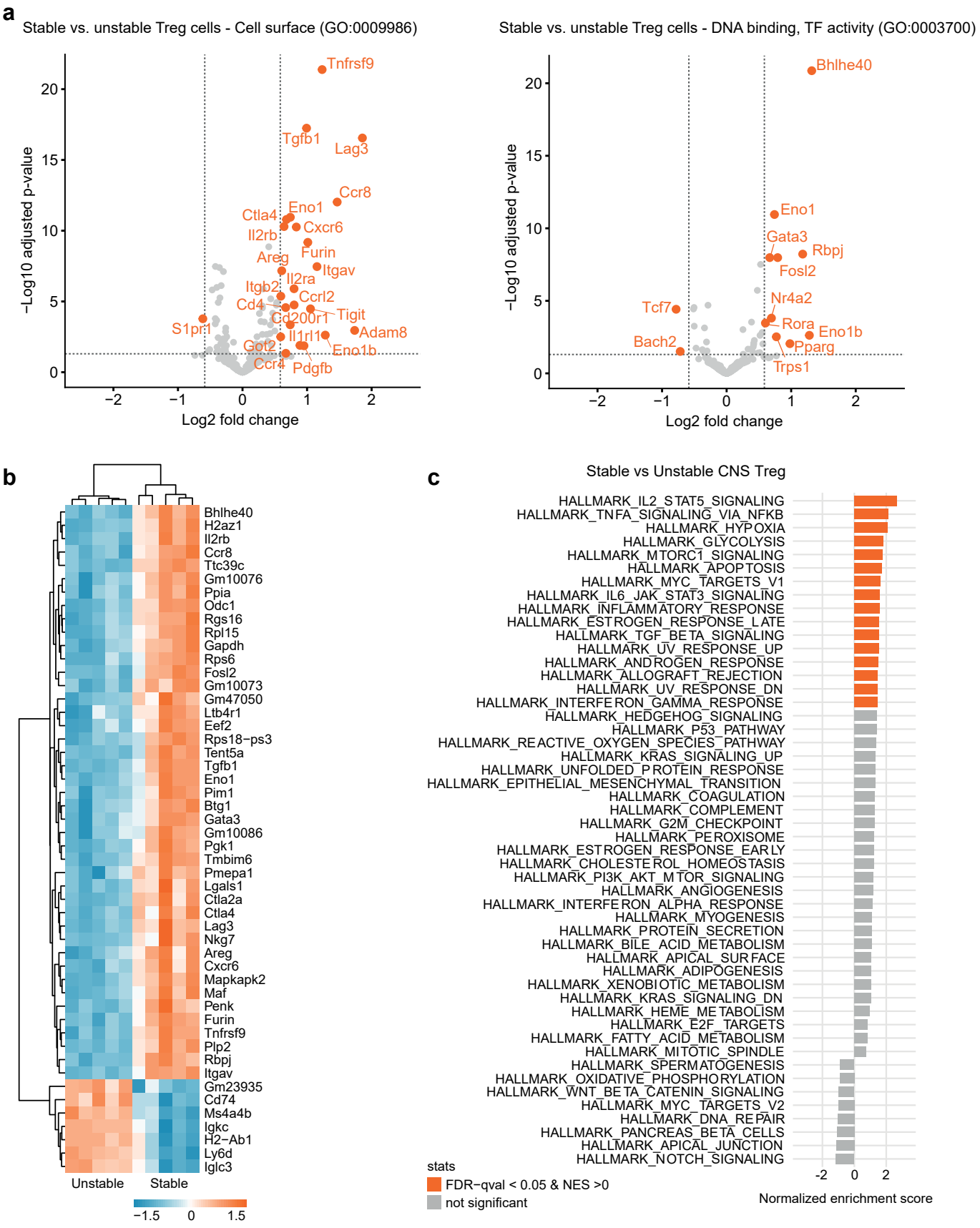

Extended Data Fig. 2 | See next page for caption.

https://doi.org/10.1038/s41590-025-02416-z

Extended Data Fig. 2 | Transcriptomic analysis of stable and unstable CNS Treg cells in chronic EAE. In vivo Foxp3 fate mapping was conducted in *Foxp3*$^{Cre\text{-}ERT2}$ x *Rosa26*$^{LSL\text{-}tdTomato}$ mice with MOG-induced EAE. Mice were injected with tamoxifen (i.p.) for 5 days at the EAE recovery stage. 14 days after the last tamoxifen injection, CNS cells were harvested and analyzed by flow cytometry. (**a**) Stable Treg cells (*Foxp3* (GFP)$^{+}$tdTomato^{+}) and unstable Treg cells (*Foxp3* (GFP)$^{-}$tdTomato^{+}) were sorted and analyzed by bulk RNA sequencing (n = 5 biological replicates). Volcano plots showing only genes with annotations to the GO terms 'GO:0009986 cell surface' and 'GO:0003700 DNA binding transcription factor activity' that exhibit differential expression (≥1.5-fold, adjusted *P* value < 0.05) between stable and unstable Treg cells. DEGs are highlighted in orange. (**b**) Heatmap showing the top 50 DEGs (≥1.5-fold, adjusted *P* value < 0.05) between stable and unstable Treg cells. Adjusted *P* values are derived from DESeq2 with a two-tailed Wald's test and correction for multiple testing using the Benjamini and Hochberg method. (**c**) Gene set enrichment analysis of MSigDB Hallmark gene sets comparing stable and unstable CNS Treg cells.

https://doi.org/10.1038/s41590-025-02416-z

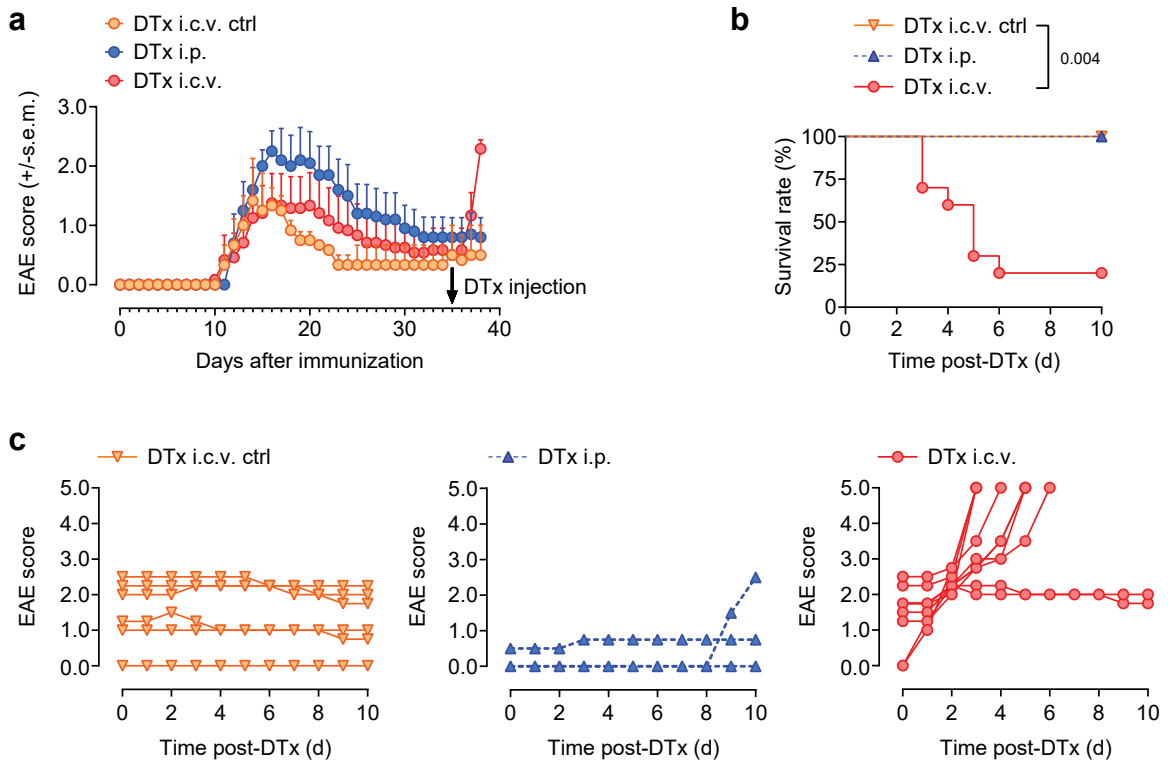

Extended Data Fig. 3 | Treg cells maintain immune homeostasis in the chronically inflamed CNS. (**a**) EAE was induced in *Foxp3* (GFP) and *Foxp3*-DTR mice. Diphtheria toxin (DTx) was administered intracerebroventricularly (i.c., 15 ng) or intraperitoneally (i.p., 500 ng) during the recovery phase of EAE. Mean EAE scores + SEM (DTx i.c. ctrl n = 3, DTx i.p. n = 5, DTx i.c. n = 6 biological replicates). (**b**) Survival of mice over 10 days following DTx injection. Survival curves were analyzed using the Mantel–Cox test (DTx i.c. ctrl n = 6, DTx i.p. n = 3, DTx i.c. n = 10 biological replicates), and corresponding individual EAE scores of mice are plotted in (**c**).

https://doi.org/10.1038/s41590-025-02416-z

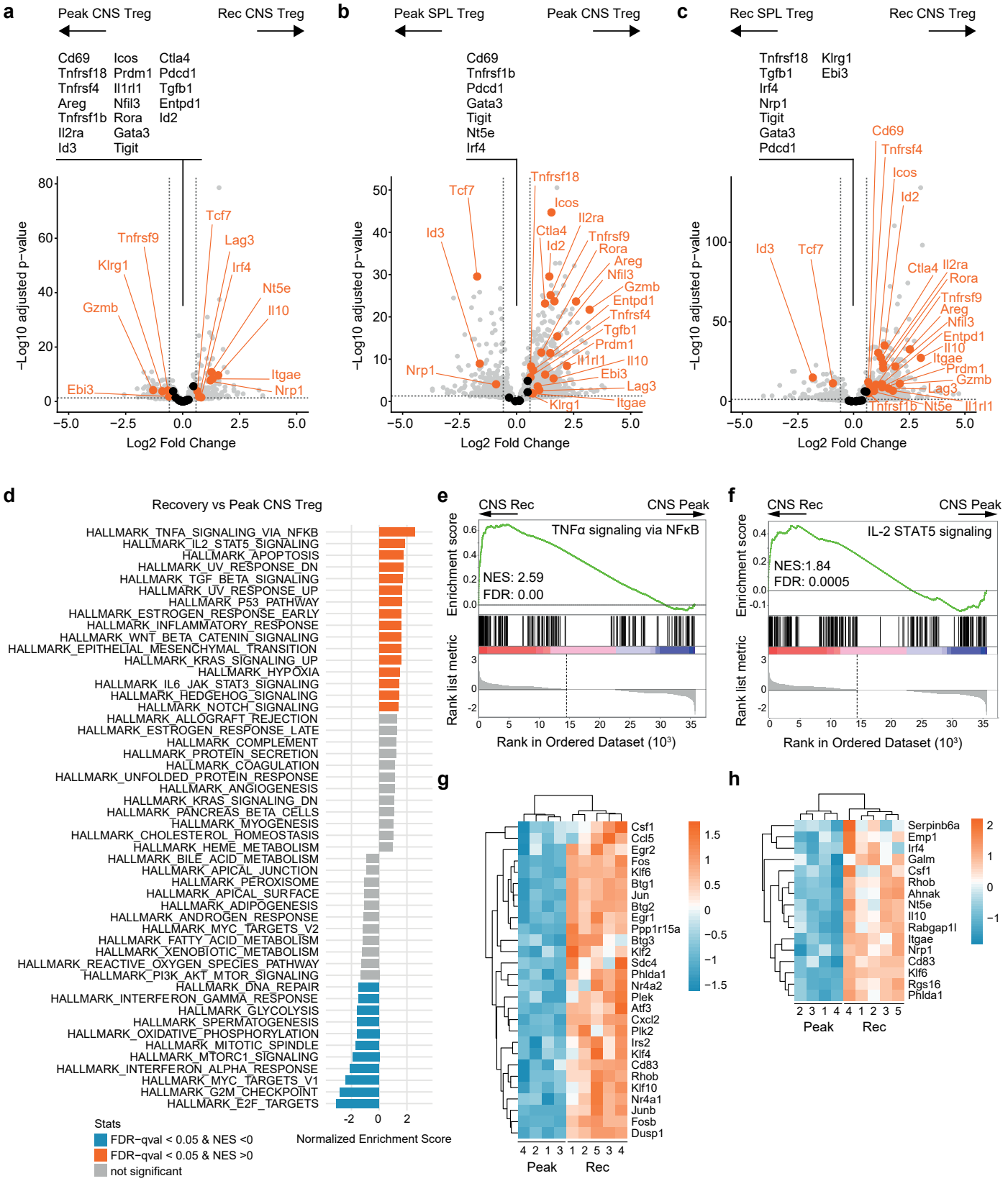

Extended Data Fig. 4 | See next page for caption.

https://doi.org/10.1038/s41590-025-02416-z

Extended Data Fig. 4 | Transcriptomic analysis of spleen and CNS Treg cells in EAE peak and recovery stages. Volcano plots displaying differentially expressed genes (≥1.5-fold, adjusted *P* value < 0.05) between recovery (Rec) and peak CNS Treg cells (**a**), peak CNS and peak spleen (SPL) Treg cells (**b**), and recovery CNS and SPL Treg cells (**c**). Adjusted *P* values in (**a**-**c**) are derived from DESeq2 using a two-tailed Wald's test with correction for multiple testing using the Benjamini and Hochberg method (peak n = 4, recovery n = 5 biological replicates). Labeled genes comprise a selection of genes commonly associated with non-nonlymphoid tissue Treg cells (black: not significantly regulated, orange: DEG, light grey: not significant and not part of the selection of tissue Treg cell genes). (**d**) Summary of gene set enrichment analyses comparing recovery and peak CNS Treg cells using the MSigDb Hallmark gene set collection. (**e, f**) Enrichment plot of genes part of the 'TNFα-signaling via NFκB' (**e**) and the 'IL-2 STAT-5 signaling' signature (FDR, false discovery rate; NES, normalized enrichment score) (**f**). (**g**-**h**) Heatmap and hierarchical clustering of significantly upregulated genes (≥1.5-fold, adjusted *P* value < 0.05) that contribute to the leading-edge genes for the gene sets 'TNFα-signaling via NFκB' (**g**) and 'IL-2 STAT-5 signaling' (**h**) in recovery (Rec) vs. peak CNS Treg cells.

https://doi.org/10.1038/s41590-025-02416-z

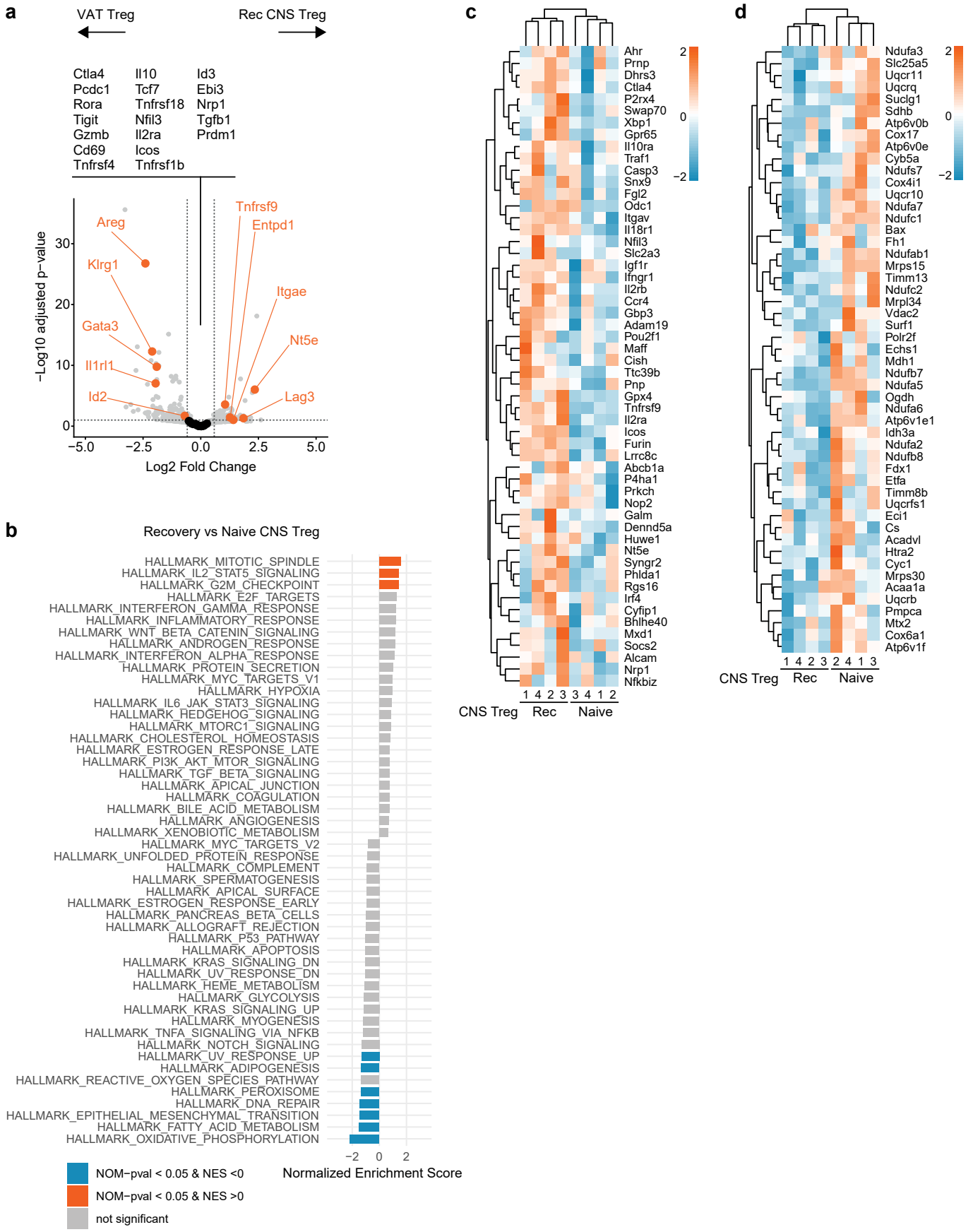

Extended Data Fig. 5 | See next page for caption.

https://doi.org/10.1038/s41590-025-02416-z

Extended Data Fig. 5 | Transcriptomic analysis of VAT and naive CNS Treg cells. (**a**) Volcano plot of differentially expressed genes (≥1.5-fold, adjusted *P* value < 0.1) of recovery (Rec) CNS Treg cells vs. VAT Treg cells. Labeled genes comprise a selection of genes commonly associated with a non-nonlymphoid tissue Treg cell phenotype (black: not significantly regulated, orange: selected DEG. Adjusted *P* values are derived from DESeq2 using a two-tailed Wald's test with correction for multiple testing using the Benjamini and Hochberg method (VAT Treg cells n = 3, recovery CNS Treg cells n = 4 biological replicates) (**b**) Summary of gene set enrichment analyses comparing recovery (Rec) CNS Treg cells from EAE mice and naive CNS Treg cells using the MSigDb Hallmark gene set collection (n = 4 biological replicates). (**c, d**) Heatmap and hierarchical clustering of genes that contribute to the leading-edge genes for the gene sets 'IL-2 STAT5 signaling' (**c**) and 'Oxidative phosphorylation' (**d**) in Rec vs. naive CNS Treg cells.

https://doi.org/10.1038/s41590-025-02416-z

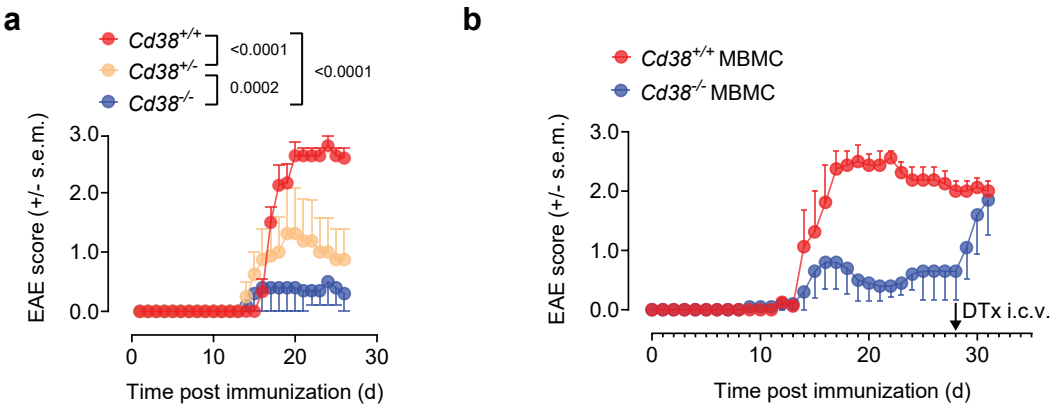

Extended Data Fig. 6 | EAE in CD38-deficient mice and MBMC mice. (**a**) EAE was induced in wild-type (*Cd38*$^{+/+}$), *Cd38*$^{+/-}$, and *Cd38*$^{-/-}$ mice. Mean EAE scores + SEM. *P* values were calculated using a two-way ANOVA with Tukey's post-test (*Cd38*$^{+/+}$ n = 6, *Cd38*$^{+/-}$ n = 4, *Cd38*$^{-/-}$ n = 5 biological replicates). (**b**) Bone marrow from *Foxp3*-DTR mice (CD45.1/2) mixed 1:1 with either *Cd38*$^{+/+}$ (CD45.2) or *Cd38*$^{-/-}$ bone marrow (CD45.2) was transferred into sublethally irradiated *Rag1*$^{-/-}$ recipients. EAE was induced in bone marrow-reconstituted mice. Diphtheria toxin (DTx) was administered intracerebroventricularly (i.c., 15 ng) in stable EAE mice on 28 days post MOG_{35-55}-immunization. Mean EAE scores + SEM (*Cd38*$^{+/+}$ MBMC n = 4, *Cd38*$^{-/-}$ MBMC n = 5 biological replicates).

https://doi.org/10.1038/s41590-025-02416-z

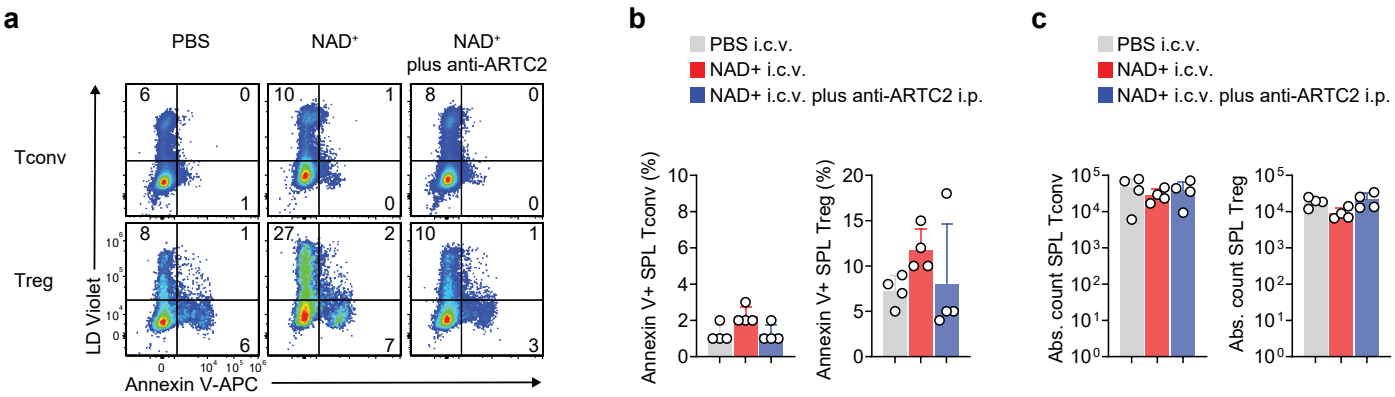

Extended Data Fig. 7 | Systemic Tconv and Treg cells are not affected by the injection of NAD$^+$ into the lateral ventricle. EAE was induced in *Foxp3* (GFP) mice. NAD$^+$ or PBS was administered intracerebroventricularly (i.c., 100 µg) with or without anti-ARTC2.2 injection (i.p., 50 µg) during the recovery stage of EAE. Mice were euthanized 1 day after treatment. Spleen (SPL) cells were isolated, and Annexin V and LD violet staining were performed on Tconv (CD4$^+$Foxp3$^-$) and Treg cells (CD4$^+$Foxp3$^+$), followed by flow cytometric analysis (**a**). (**b**) Percentage of Annexin V$^+$ and (**c**) total counts of viable (Annexin V$^-$LD violet$^-$) splenic Tconv and Treg cells. Symbols in (**b, c**) represent individual mice (n = 4 biological replicates).

https://doi.org/10.1038/s41590-025-02416-z

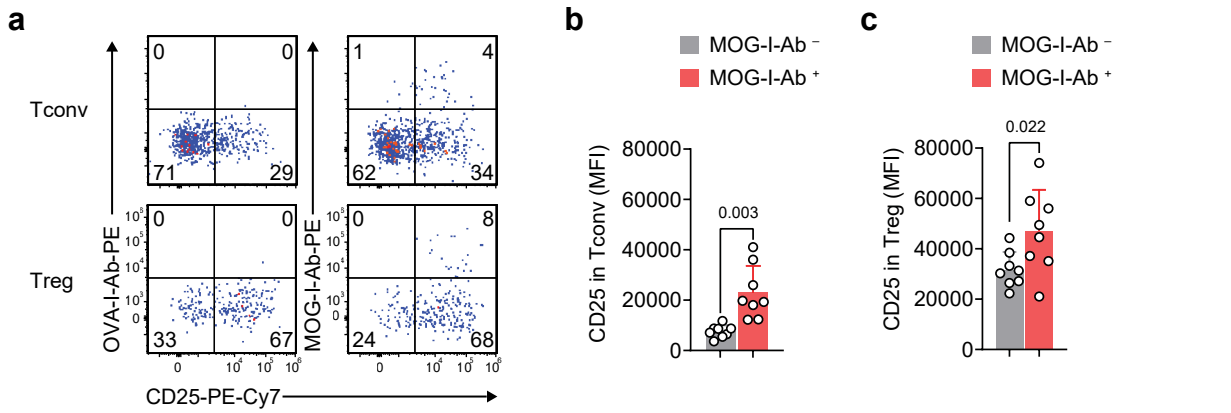

Extended Data Fig. 8 | Antigen-specific Tconv and Treg cells express higher levels of CD25. EAE was induced in *Foxp3* (GFP) mice, and CNS cells were collected during the EAE recovery stage. (**a**) The percentage of CD25 expression was determined in MOG-I-Ab tetramer-binding Tconv and Treg cells. An $OVA_{323-339}$ -I-Ab tetramer was used as a control tetramer. CD25 expression (MFI) in MOG-I-Ab$^-$ vs. MOG-I-Ab$^+$ Tconv (**b**) and Treg cells (**c**). Symbols in (**b, c**) represent individual mice. Data are means + s.d. *P* values were calculated using a paired two-tailed Student's t-test (n = 8 biological replicates).

nature portfolio

Corresponding author(s): Thomas Korn

Last updated by author(s): Jan 13, 2026

Reporting Summary

Nature Portfolio wishes to improve the reproducibility of the work that we publish. This form provides structure for consistency and transparency in reporting. For further information on Nature Portfolio policies, see our Editorial Policies and the Editorial Policy Checklist.

Statistics

For all statistical analyses, confirm that the following items are present in the figure legend, table legend, main text, or Methods section.

n/a	Confirmed	
☐	☒	The exact sample size (*n*) for each experimental group/condition, given as a discrete number and unit of measurement
☐	☒	A statement on whether measurements were taken from distinct samples or whether the same sample was measured repeatedly
☐	☒	The statistical test(s) used AND whether they are one- or two-sided *Only common tests should be described solely by name; describe more complex techniques in the Methods section.*
☐	☒	A description of all covariates tested
☐	☒	A description of any assumptions or corrections, such as tests of normality and adjustment for multiple comparisons
☐	☒	A full description of the statistical parameters including central tendency (e.g. means) or other basic estimates (e.g. regression coefficient) AND variation (e.g. standard deviation) or associated estimates of uncertainty (e.g. confidence intervals)
☐	☒	For null hypothesis testing, the test statistic (e.g. *F*, *t*, *r*) with confidence intervals, effect sizes, degrees of freedom and *P* value noted *Give P values as exact values whenever suitable.*
☒	☐	For Bayesian analysis, information on the choice of priors and Markov chain Monte Carlo settings
☒	☐	For hierarchical and complex designs, identification of the appropriate level for tests and full reporting of outcomes
☒	☐	Estimates of effect sizes (e.g. Cohen's *d*, Pearson's *r*), indicating how they were calculated

Our web collection on statistics for biologists contains articles on many of the points above.

Software and code

Policy information about availability of computer code

Data collection	CytoFLEX (Beckman Coulter), FACSAria™ III (BD Biosciences), Aurora (Cytek Biosciences), Illumina NextSeq 500 platform, SP8 confocal microscope (Leica), Leica AT2 system (Leica), Akoya PhenoImager HT 2.0 (Akoya Biosciences), SP8 confocal microscope (Leica)
Data analysis	R (v4.4.0), DESeq2 package (v1.44.0), glmGamPoi (v1.16.0), org.Mm.eg.db (v3.19.1), GSEA Desktop Application (v4.3.2), Molecular Signatures Database (v2024.1.Mm), FlowJo software (v10.8.1, BD Biosciences), FlowSOM (v3.0.18), ClusterExplorer (v1.6.5), QuPath (v0.6.0) , LAS X software (v.3.5.6.21594), LAS X software (v.3.5.6.21594, Leica), Prism (v10, GraphPad).

For manuscripts utilizing custom algorithms or software that are central to the research but not yet described in published literature, software must be made available to editors and reviewers. We strongly encourage code deposition in a community repository (e.g. GitHub). See the Nature Portfolio guidelines for submitting code & software for further information.

Data

Policy information about availability of data

All manuscripts must include a data availability statement. This statement should provide the following information, where applicable:

- Accession codes, unique identifiers, or web links for publicly available datasets
- A description of any restrictions on data availability
- For clinical datasets or third party data, please ensure that the statement adheres to our policy

Data availability: All sequencing data were deposited with the GEO database. Accession number: GSE311963.

RNA-seq Data processing: The GRCm38 reference genome was aligned with transcript and gene annotations derived from ENSEMBL release 75. Differential gene expression analysis was conducted in R (v4.4.0) using the DESeq2 package (v1.44.0). Significant differentially expressed genes (DEG) were defined as genes with a Benjamini-Hochberg (BH)-adjusted p-value < 0.05 or 0.1, labeled in the legends, and an absolute fold change in expression of >1.5. Log2 fold shrinkage estimation was performed using the R package glmGamPoi (v1.16.0). Gene ontology (GO) term annotations were derived from the R package org.Mm.eg.db (v3.19.1).
RNA-seq Data visualization: Count data were transformed using the variance stabilizing transformation ("vst") function in DESeq2. Gene Set Enrichment Analysis (GSEA) was performed on DESeq2 normalized counts using the Broad Institute GSEA Desktop Application (v4.3.2) in conjunction with the Molecular Signatures Database (v2024.1.Mm), with permutation type "gene_set" and a false discovery rate (FDR) threshold of 0.25 applied.
Flow result visualizations: An analysis was performed to identify Treg cells through primary gating in FlowJo, defining each sample's Treg cell (Aqua–Foxp3+CD4+) population. To standardize cell numbers across tissues, downsampling was conducted by pooling and selecting 300 Treg cells, which were then subjected to secondary FlowSOM (v3.0.18) clustering. Further sub-clustering of Treg cells was achieved using ClusterExplorer (v1.6.5). The clusters were visualized with UMAP through R and the FlowJo Plugin packages.

Research involving human participants, their data, or biological material

Policy information about studies with human participants or human data. See also policy information about sex, gender (identity/presentation), and sexual orientation and race, ethnicity and racism.

Reporting on sex and gender	No human sample used in this study.
Reporting on race, ethnicity, or other socially relevant groupings	*Please specify the socially constructed or socially relevant categorization variable(s) used in your manuscript and explain why they were used. Please note that such variables should not be used as proxies for other socially constructed/relevant variables (for example, race or ethnicity should not be used as a proxy for socioeconomic status).* *Provide clear definitions of the relevant terms used, how they were provided (by the participants/respondents, the researchers, or third parties), and the method(s) used to classify people into the different categories (e.g. self-report, census or administrative data, social media data, etc.)* *Please provide details about how you controlled for confounding variables in your analyses.*
Population characteristics	*Describe the covariate-relevant population characteristics of the human research participants (e.g. age, genotypic information, past and current diagnosis and treatment categories). If you filled out the behavioural & social sciences study design questions and have nothing to add here, write "See above."*
Recruitment	*Describe how participants were recruited. Outline any potential self-selection bias or other biases that may be present and how these are likely to impact results.*
Ethics oversight	*Identify the organization(s) that approved the study protocol.*

Note that full information on the approval of the study protocol must also be provided in the manuscript.

Field-specific reporting

Please select the one below that is the best fit for your research. If you are not sure, read the appropriate sections before making your selection.

☒ Life sciences ☐ Behavioural & social sciences ☐ Ecological, evolutionary & environmental sciences

For a reference copy of the document with all sections, see nature.com/documents/nr-reporting-summary-flat.pdf

Life sciences study design

All studies must disclose on these points even when the disclosure is negative.

Sample size	This study is exploratory and no statistical methods were applicable to predict the sample size. The sample size is determined to be sufficient based on established standard for exploitative study in this field.
Data exclusions	All replication attempts with matching preoperative disease status were included in the analysis.
Replication	All of the experiments were repeated at least twice with several biological replications per group to ensure reproducibility.
Randomization	Randomization was not applicable in this study. Mice were matched for age and disease stages before undergoing the procedure to evaluate treatment effects.
Blinding	Whenever possible, EAE scoring was performed by more than two experienced staff members (in a blinded manner). Furthermore, the data analysis in this study was quantitative rather than subjective.

Reporting for specific materials, systems and methods

We require information from authors about some types of materials, experimental systems and methods used in many studies. Here, indicate whether each material, system or method listed is relevant to your study. If you are not sure if a list item applies to your research, read the appropriate section before selecting a response.

Materials & experimental systems

n/a	Involved in the study
☐	☒ Antibodies
☒	☐ Eukaryotic cell lines
☒	☐ Palaeontology and archaeology
☐	☒ Animals and other organisms
☒	☐ Clinical data
☒	☐ Dual use research of concern
☒	☐ Plants

Methods

n/a	Involved in the study
☒	☐ ChIP-seq
☐	☒ Flow cytometry
☒	☐ MRI-based neuroimaging

Antibodies

Antibodies used

Antibodies
IHC:
Peroxidase labeled polymer conjugated to goat anti-rabbit IgG,Agilent Cat# K4003, RRID:AB_2630375, (1:500)
ImmPRESS Anti-Rat Ig (Mouse Adsorbed) Reagent, Vector Laboratories Cat# MP-7444, RRID:AB_2336530, (1:500)
FOXP3 Monoclonal Antibody (FJK-16s), PE-Cyanine5, eBioscience, Thermo Fisher Scientific Cat# 15-5773-82, RRID:AB_468806, (1:50)
CD4 (D7D2Z) Rabbit mAb, Cell Signaling Technology Cat# 25229, RRID:AB_2798898, (1:100)
Goat Anti-Rabbit IgG H&L (Alexa Fluor 647) preadsorbed, Abcam Cat# ab150087, RRID:AB_ 3095880, (1:500)
CD4 [EPR6855], Abcam Cat# ab133616, RRID:AB_ 2750883, (1:500)
Anti Ibal, Monoclonal Antibody (NCNP24), FUJIFILM Wako Pure Chemical Corporation Cat# 016-26721, RRID:AB_2811160, (1:500)
CD4 Monoclonal Antibody (4SM95) eBioscience, Thermo Fisher Scientific Cat# 14-9766-80, RRID:AB_2573007, (1:500)
Rat Anti-Mouse CD45 (30-F11) Monoclonal, Unconjugated, Clone 30-f11, Santa Cruz Biotechnology Cat# sc-53665, RRID:AB_629093. (1:200)
Flow cytometry analysis:
APC/Fire 750 anti-mouse CD62L, BioLegend Cat# 104450, RRID:AB_2629772, (1:400)
CD103, BD Biosciences Cat# 565529, RRID:AB_2739282, (1:250)
Alexa Fluor 647 anti-mouse CD186 (CXCR6), BioLegend Cat# 151115, RRID:AB 2721358, (1:250)
APC anti-mouse CD184 (CXCR4), BioLegend Cat# 146508, RRID:AB 2562785, (1:250)
PE/Dazzle 594 anti-mouse TIGIT (Vstm3), BioLegend Cat# 142109, RRID:AB_2566572, (1:250)
IL-33R (ST2) Monoclonal Antibody (RMST2-2) PE, eBioscience, Thermo Fisher Scientific Cat# 12-9335-82, RRID:AB_2572708, (1:250)
CD4 Monoclonal Antibody (RM4-5), Alexa Fluor 532, eBioscience, Thermo Fisher Scientific Cat# 58-0042-82, RRID:AB_11218891, (1:500)
Brilliant Violet 785 anti-mouse/human KLRG1 (MAFA), BioLegend Cat# 138429, RRID:AB_2629749, (1:250)
CD27, BD Biosciences Cat# 740699, RRID:AB_2740383CD44, BD Biosciences Cat# 563058, RRID:AB_2737979, (1:250)
Brilliant Violet 650 anti-mouse/human CD44, BioLegend Cat# 103049, RRID:AB_2562600, (1:400)
FR4 (Folate Receptor 4), BD Biosciences Cat# 746345, RRID:AB_2743664, (1:400)
CD25 Monoclonal Antibody (PC61.5), eFluor 450, eBioscience, Thermo Fisher Scientific Cat# 48-0251-82, RRID:AB_10671550, (1:250)
Brilliant Violet 421 anti-mouse CD304 (Neuropilin-1), BioLegend Cat# 145209, RRID:AB_2562358, (1:250)
Treg-Protector (anti-ARTC2 Nanobody), BioLegend Cat# 149802, RRID:AB_2565494, (1:1000)
Purified Rat Anti-Mouse CD16/CD32 (Mouse BD Fe Blocker) Clone 2.4G2, BD Biosciences Cat# 553141, RRID:AB_394656, (1:250)
CD4 Monoclonal Antibody (GK1.5), APC-eFluor 780, eBioscience, Thermo Fisher Scientific Cat# 47-0041-82, RRID:AB_11218896, (1:500)
Anti-Mouse F4/80 Antigen APC-eFluor 780, Thermo Fisher Scientific Cat# 47-4801, RRID:AB_1548745, (1:500)
APC/Cyanine7 anti-mouse Ly-6G, BioLegend Cat# 127624, RRID:AB 10640819, (1:500)
APC/Cyanine7 anti-mouse CD8a, BioLegend Cat# 100713, RRID:AB_312752, (1:500)
CD19,BD Biosciences Cat# 561737, RRID:AB_10896279, (1:500)
Alexa Fluor 700 anti-mouse CD4, BioLegend Cat# 100536, RRID:AB_493701, (1:500)
Alexa Fluor 647 anti-mouse CD69, BioLegend Cat# 104518, RRID:AB 492847, (1:250)
Annexin V Recom APC, BD Biosciences Cat# 550475, RRID:AB_2868885, (1:250)
Phospho-STATS (Tyr694) Monoclonal Antibody (SRBCZX), APC, eBioscience, Thermo Fisher Scientific Cat# 17-9010-42, RRID:AB_2573272, (1:200)
APC anti-mouse CD357 (GITR), BioLegend Cat# 126312, RRID:AB_2271858, (1:250)
CD45.2 Monoclonal Antibody (104), APC, eBioscience, Thermo Fisher Scientific Cat# 17-0454-82, RRID:AB_469400, (1:400)
FOXP3 Monoclonal Antibody (FIK-16s), PE-Cyanine7, eBioscience, Thermo Fisher Scientific Cat# 25-5773-82, RRID:AB_891552,(1:200)
Rat Anti-Mouse CD25 Monoclonal Antibody, PE Conjugated, Clone 7D4, BD Biosciences Cat# 558642, RRID:AB_1645250, (1:250)
CD38 Monoclonal Antibody (90), PerCP-eFluor 710, eBioscience, Thermo Fisher Scientific Cat# 46-0381-82, RRID:AB_10853677, (1:250)
CD4 Monoclonal Antibody (RM4-5), PerCP-eFluor 710, eBioscience, Thermo Fisher Scientific Cat# 46-0042-82, RRID:AB_1834431, (1:500)
Armenian Hamster Anti-CD69 Monoclonal Antibody, PerCP-Cy5.5 Conjugated, Clone H1.2F3, BD Biosciences Cat# 551113, RRID:AB_394051, (1:200)
CD4 Monoclonal Antibody (RM4-5), Alexa Fluor 532, eBioscience, Thermo Fisher Scientific Cat# 58-0042-80, RRID:AB_11219484, (1:500)
CD25, BD Biosciences Cat# 553071, RRID:AB_394603, (1:250)
FOXP3 Monoclonal Antibody (FIK-16s), Alexa Fluor 488, eBioscience, Thermo Fisher Scientific Cat# 53-5773-82, RRID:AB_763537, (1:250)
Alexa Fluor 488 anti-mouse CD38, BioLegend Cat# 102714, RRID:AB_528796, (1:250)
Brilliant Violet 711 anti-mouse TCR beta chain, BioLegend Cat# 109243, RRID:AB_2629564, (1:400)
Brilliant Violet 650 anti-mouse CD45.2, BioLegend Cat# 109836, RRID:AB_2563065, (1:400)

Brilliant Violet 650 anti-mouse CD45.1, BioLegend Cat# 110736, RRID:AB_2562564, (1:400)
CD38 Monoclonal Antibody (90), eFluor 450, eBioscience, Thermo Fisher Scientific Cat# 48-0381-82, RRID:AB_11218302, (1:250)
CD25 Monoclonal Antibody (PC61.5), eFluor 450, eBioscience, Thermo Fisher Scientific Cat# 48-0251-80, RRID:AB_10698312
P2X7, BD Biosciences Cat# 744779, RRID:AB_2742477, (1:250)
Brilliant Violet 421 anti-mouse CD45.1, BioLegend Cat# 110732, RRID:AB_ 2562563, (1:400)
Tetramer:
T-Select I-Ab MOG35-55 Tetramer-PE (Medical & Biological Laboratories Cat# TS-M704-1), (1:60)
T-Select I-Ab OVA323-339 Tetramer-PE (Medical & Biological Laboratories Cat# TS-M710-1), (1:60)

Validation

All antibodies used in this study are commercially available and have been widely validated by either the suppliers or other researchers. In addition, biological controls were performed using cells known to lack the relevant antigens.

Animals and other research organisms

Policy information about studies involving animals; ARRIVE guidelines recommended for reporting animal research, and Sex and Gender in Research

Laboratory animals

Foxp3eGFP-Cre-ERT2 (Foxp3ERT2-Cre, IMSR_JAX:016961), Foxp3DTR (Fxop3DTR, IMSR_JAX:016958), Rag1-/- (IMSR_JAX:002216), CD45.1 (IMSR_JAX:002014) mice were obtained from Jackson Laboratory. C57BL/6J (WT, IMSR_JAX:000664) mice were from Charles River Laboratories. Foxp3 (GFP) reporter mice were provided by Vijay Kuchroo (Harvard Medical School and Brigham and Women's Hospital, USA). Cd38tm1Lnd (CD38–/–, IMSR_JAX:003727) mice were provided by Hans-Willi Mittrücker (Medical Center Hamburg-Eppendorf, Germany).Foxp3eGFP-Cre-ERT2 (from Jackson Laboratory) and Rosa-CAG-LSL-tdTomato-WPRE::ΔNeo (Rosa26LSL-tdTomato, IMSR_JAX:007914) mice, provided by Marc Schmidt-Supprian (Technical University of Munich, Germany), were mated to generate Foxp3eGFP-Cre-ERT2-Cre Rosa26-LSL-tdTomato mice.CD4-Cre Phamfloxed (CD4-Cre-mitoDendra2, IMSR_JAX:022071 mated with IMSR_JAX:018385) reporter mice were generated in-house. DEREG (MMRRC_032049-JAX) mice were provided by Tim Sparwasser (University Medical Center Mainz, Germany).
All mice were in C57BL/6 background, and 8-20-age old mice. They all housed with normal chow in a specific pathogen-free facility at the Technical University of Munich.

Wild animals

No wild animal is used in this study.

Reporting on sex

We did not observe any impact of sex on disease progression, and previous evidence indicates that sex does not affect disease development in this animal model. Therefore, both male and female mice were included in the study, except for the visceral adipose tissue which was exclusively derived from male mice.

Field-collected samples

No field-collected sample is used in this study.

Ethics oversight

The animal protocols were approved by the Bavarian state authorities and conducted in accordance with relevant guidelines (ROB-55.2-2532.Vet_02-17-69, ROB-55.2-2532.Vet_02-17-234, ROB-55.2-2532.Vet_03-18-53, ROB-55.2-2532.Vet_02-20-1, ROB-55.2-2532.Vet_02-20-23, ROB-55.2-2532.Vet_02-20-187, ROB-55.2-2532.Vet_02-23-71, ROB-55.2-2532.Vet_02-23-118, ROB-55.2-2532.Vet_02-25-68).

Note that full information on the approval of the study protocol must also be provided in the manuscript.

Plants

Seed stocks

No plant sample used in this study.

Novel plant genotypes

Describe the methods by which all novel plant genotypes were produced. This includes those generated by transgenic approaches, gene editing, chemical/radiation-based mutagenesis and hybridization. For transgenic lines, describe the transformation method, the number of independent lines analyzed and the generation upon which experiments were performed. For gene-edited lines, describe the editor used, the endogenous sequence targeted for editing, the targeting guide RNA sequence (if applicable) and how the editor was applied.

Authentication

Describe any authentication procedures for each seed stock used or novel genotype generated. Describe any experiments used to assess the effect of a mutation and, where applicable, how potential secondary effects (e.g. second site T-DNA insertions, mosiacism, off-target gene editing) were examined.

Flow Cytometry

Plots

Confirm that:

☒ The axis labels state the marker and fluorochrome used (e.g. CD4-FITC).

☒ The axis scales are clearly visible. Include numbers along axes only for bottom left plot of group (a 'group' is an analysis of identical markers).

☒ All plots are contour plots with outliers or pseudocolor plots.

☒ A numerical value for number of cells or percentage (with statistics) is provided.

Methodology

Sample preparation	Cell suspensions were stained with Live/Dead Aqua, Live/Dead violet, or Near-IR dyes (Thermo Fisher) for 15 minutes at 4°C in PBS and washed with FACS buffer. Cells were incubated with an antibody cocktail targeting surface antigen and CD16/CD32 Fc-block in FACS buffer for 15 minutes at 4°C in the dark, washed twice, and resuspended in FACS buffer. For Annexin V staining, cells were stained with an antibody cocktail in the Annexin V binding buffer (BioLegend). For intracellular staining, cells were stained with antibodies against surface antigens, then fixed with 4% PFA for 15 minutes at room temperature, protected from light, and washed with FACS buffer. Fixation and permeabilization were performed using the eBioscience Intracellular Fixation & Permeabilization Buffer Set (Invitrogen). Cells were incubated overnight at 4 °C with an intracellular antibody cocktail and Fc-block in permeabilization buffer, washed, and resuspended in FACS buffer. For phosphorylated Stat5Y694 (pStat5Y694) staining, fixation and permeabilization were performed using Transcription Factor Phospho Buffer Set (TFP, BD Pharmingen™) following the manufacturer's protocol. In short, after the fixation and permeabilization, the cells were incubated with anti-pStat5 Y694, anti-Foxp3, and anti-surface antigen antibody cocktail with Fc-block in TFP Perm/Wash Buffer for 50 min at 4 °C. Wash cells twice with TFP Perm/Wash Buffer and resuspend in FACS buffer for flow cytometry analysis.
Instrument	CytoFLEX (Beckman Coulter), FACSAria™ III (BD Biosciences), Aurora (Cytek Biosciences)
Software	CytExpert (v.2.4), BD FACSDIVA (v.9.0), SpectroFlo CS (v.1.4.1), FlowJo software (v10.8.1, BD Biosciences)
Cell population abundance	Cell sorting was performed with FACSAria™ III and used 4-way purity to ensure purity >95%.
Gating strategy	The detailed gating strategies are provided in the individual figure legends, according to the specific analytical purpose. In general, debris and dead cells were excluded using live/dead staining and SSC/FSC gating. Conventional T cells (Tconv; $CD4^+Foxp3^-$ or $CD4^+CD25^-GITR^-$) and regulatory T cells (Treg; $CD4^+Foxp3^+$ or $CD4^+CD25^+GITR^+$) were then gated for further analysis.

☒ Tick this box to confirm that a figure exemplifying the gating strategy is provided in the Supplementary Information.